Responses of Basal Melting of Antarctic Ice Shelves to the Climatic Forcing of the Last Glacial Maximum and CO_2 Doubling

TAKASHI OBASE

Atmosphere and Ocean Research Institute, University of Tokyo, Kashiwa, Japan

AYAKO ABE-OUCHI

Atmosphere and Ocean Research Institute, University of Tokyo, Kashiwa, and Japan Agency for Marine-Earth Science and Technology, Yokohama, Japan

KAZUYA KUSAHARA

Antarctic Climate and Ecosystems Cooperative Research Centre, University of Tasmania, Hobart, Tasmania, Australia, and Atmosphere and Ocean Research Institute, University of Tokyo, Kashiwa, Japan

HIROYASU HASUMI

Atmosphere and Ocean Research Institute, University of Tokyo, Kashiwa, Japan

RUMI OHGAITO

Japan Agency for Marine-Earth Science and Technology, Yokohama, Japan

(Manuscript received 19 December 2015, in final form 24 January 2017)

ABSTRACT

Basal melting of the Antarctic ice shelves is an important factor in determining the stability of the Antarctic ice sheet. This study used the climatic outputs of an atmosphere–ocean general circulation model to force a circumpolar ocean model that resolves ice shelf cavity circulation to investigate the response of Antarctic ice shelf melting to different climatic conditions (i.e., to a doubling of CO_2 and to the Last Glacial Maximum conditions). Sensitivity experiments were also conducted to investigate the roles of both surface atmospheric change and changes of oceanic lateral boundary conditions. It was found that the rate of change of basal melt due to climate warming is much greater (by an order of magnitude) than that due to cooling. This is mainly because the intrusion of warm water onto the continental shelves, linked to sea ice production and climate change, is crucial in determining the basal melt rate of many ice shelves. Sensitivity experiments showed that changes of atmospheric heat flux and ocean temperature are both important for warm and cold climates. The offshore wind change, together with atmospheric heat flux change, strongly affected the production of both sea ice and high-density water, preventing warmer water approaching the ice shelves under a colder climate. These results reflect the importance of both water mass formation in the Antarctic shelf seas and subsurface ocean temperature in understanding the long-term response to climate change of the melting of Antarctic ice shelves.

1. Introduction

Understanding the nature and stability of the Antarctic ice sheet is important when projecting future rises in sea level (Church et al. 2013; Clark et al. 2016). Most of the western region of the Antarctic ice sheet is grounded below sea level and fringed by floating ice shelves (Fretwell et al. 2013); therefore, it could be particularly vulnerable to the effects of climate forcing because of the instability of the marine ice sheet (Weertman 1974; Schoof 2007). Climate can affect the ice sheet directly via changes in atmospheric temperature and precipitation, but the primary mechanism is through local ocean temperature change near the ice shelves. Recent observations have revealed mass loss of

Corresponding author e-mail: Takashi Obase, obase@aori.u-tokyo.ac.jp

DOI: 10.1175/JCLI-D-15-0908.1

the Antarctic ice sheet and thinning of the ice shelves (Pritchard et al. 2009; Velicogna 2009; Pritchard et al. 2012). Furthermore, geological surveys have elucidated historical variations in the extent of the Antarctic ice sheet under climatic conditions both warmer and colder than the present, represented by the Last Interglacial period and the Pliocene (Kopp et al. 2009; Naish et al. 2009; Dutton and Lambeck 2012; Cook et al. 2013; Masson-Delmotte et al. 2013; Suganuma et al. 2014; Dutton et al. 2015; Yamane et al. 2015; McKay et al. 2016) and the Last Glacial Maximum (LGM), respectively (Bentley et al. 2014; Abe-Ouchi et al. 2015; Peltier et al. 2015). Numerical ice sheet models have been used to reconstruct the shapes of ice sheets and to investigate their responses to variations in climate forcing (Abe-Ouchi et al. 2013; de Boer et al. 2013). In Antarctica, basal ice shelf melting and calving are the two important processes that determine the mass balance of the ice sheet (Depoorter et al. 2013; Rignot et al. 2013). Studies modeling the Antarctic ice sheet have shown that an increase in basal melting plays an essential role in the retreat of the marine ice sheet (Pollard and DeConto 2009; Golledge et al. 2012; Sato and Greve 2012; Bindschadler et al. 2013; de Boer et al. 2013; Golledge et al. 2014). This is because the loss of the ice shelves reduces ice-shelf buttressing, which affects the flow of the continental ice sheet (Dupont and Alley 2005; Schoof 2006; Walker et al. 2008; Gagliardini et al. 2010).

Modeling of the Antarctic ice sheet requires the basal melt rates of the ice shelves as boundary conditions. Physically, basal melting occurs because of heat delivered from the ocean beneath the ice shelves (Hellmer and Olbers 1989). Glaciological surveys have indicated that high rates of basal melting occur currently in the western part of Antarctica, concentrated on the grounding lines (Rignot and Jacobs 2002; Rignot et al. 2013). The observed differences in basal melt rates among various regions reflect the differences in the basal melting mode and ocean temperature of the Antarctic shelf seas (Jacobs et al. 1992). The first mode is characterized by a low rate of basal melting, driven by the thermohaline circulation due to sea ice production and the formation of high-salinity shelf water (with a temperature of ~ -1.9°C) (Jacobs et al. 1985; Nicholls 1997; Morales Maqueda et al. 2004). In contrast, the second mode of basal melting is characterized by a very high rate of melting (Talbot 1988; Jacobs et al. 1996; Jenkins and Jacobs 2008; Jacobs et al. 2011) due to the flow onto the continental shelves of warm (~1°C) and saline Circumpolar Deep Water (CDW) originating from the Southern Ocean. Generally, the steep topography at the continental shelf break limits the inflow of CDW onto the continental shelves; however, eddies generated by the seafloor topography (St-Laurent et al. 2013), tides (Dinniman et al. 2011), and winds around the continental shelf break (Thoma et al. 2008) are proposed for the transport of warm water onto the continental shelves. The third mode of basal melting is characterized by summertime melting in the frontal area of the ice shelf because of the formation of seasonal warm water (Jacobs et al. 1985), as observed in the Ross Sea. One exception, which could be considered another mode, is characterized by low basal melting due to easterly winds and the subduction of cold surface water along the Antarctic coast, which prevents warm subsurface water from flowing into ice shelf cavities (Whitworth et al. 1998; Nøst et al. 2011; Hattermann et al. 2012).

Ocean models with an ice shelf cavity component are needed to investigate the response of ice shelf melting to changes in boundary conditions (Hellmer 2004; Losch 2008; Galton-Fenzi et al. 2012; Miller et al. 2012; Timmermann et al. 2012; Dinniman et al. 2015; Kusahara et al. 2015). The response of ice shelf melting to subsurface ocean warming in front of the ice shelf has been investigated in previous research (Hellmer et al. 1998; Williams et al. 1998; Holland et al. 2008). However, its response to climate change is affected not only by subsurface ocean temperature but also by sea surface-driven water mass formation in the Antarctic shelf seas. Ocean models have shown that sea ice production and the formation of cold and dense water masses in the Antarctic shelf seas affect the intrusion of warm water onto the Antarctic continental shelves (Petty et al. 2013; Timmermann and Hellmer 2013). Kusahara and Hasumi (2013) systematically applied air temperature anomalies of 1°–6°C and they discussed the changing properties of the water masses flowing into the ice shelf cavities. Hellmer et al. (2012) and Timmermann and Hellmer (2013) used atmosphere–ocean general circulation models (AOGCMs) with CO_2 emission scenarios of the Intergovernmental Panel on Climate Change to force an ocean model to project the basal melt rates of Antarctic ice shelves in the twenty-first and twenty-second centuries. They showed that drastic increases in both the seawater temperature of the shelf seas and the basal melt rate of the ice shelves occur because a reduction in the extent of sea ice and convection leads to the flow of warm water onto the continental shelves and into the ice shelf cavities.

To project future climate change and the associated response of the Antarctic ice sheet, it is necessary to couple an ice sheet model and an AOGCM (Holland and Holland 2015; Kusahara 2016) and to adopt a long-term

perspective because of the inertia of the climate system (Clark et al. 2016). Previous studies have used Antarctic subsurface ocean temperatures (Beckmann and Goosse 2003) derived from an AOGCM to parameterize the basal mass balance beneath the ice shelves in their ice sheet models (de Boer et al. 2015; Golledge et al. 2015; Sutter et al. 2016; Deconto and Pollard 2016). Subsurface ocean temperature near ice shelves is generally assumed to be the same as the ocean temperature beyond the continental shelf break because AOGCMs have insufficient horizontal resolution to resolve water mass formation in the Antarctic continental shelf seas. Future projections have indicated the importance to the basal melt rate of ice sheets of resolving water mass formation in the shelf seas (Hellmer et al. 2012; Timmermann and Hellmer 2013). However, some of the most recent ice sheet modeling studies used an ocean model to project the future loss of the Antarctic ice sheet (Gong et al. 2014; Mengel and Levermann 2014; Mengel et al. 2015). They used an ocean model, capable of resolving Antarctic ice shelf cavity circulations over the next two centuries, forced by an AOGCM (Timmermann and Hellmer 2013). These generated data were then used as inputs for the basal mass balance of the ice shelves in ice sheet models.

The objective of this paper is to understand the important processes that determine the long-term responses of both ocean temperature in the Antarctic shelf seas and basal melt rate of the Antarctic ice shelves to atmospheric and oceanic fields simulated by an AOGCM. We use an AOGCM and a circumpolar ocean model that resolves ice shelf cavity circulations to investigate the response of the basal melt rate of the Antarctic ice shelf. We simulate the climates of the LGM and a quasi-equilibrium CO_2 doubling ($2\times CO_2$) as representatives of extreme colder and warmer conditions, respectively, which are often referred to as benchmarks among paleoclimate modeling studies and future projections (Braconnot et al. 2007; Yoshimori et al. 2009). A challenge in simulating the Antarctic ice sheet at the LGM is that both the climatic conditions and the Antarctic ice shelf configuration affect the basal melt rate, as simulated by Kusahara et al. (2015) using the same circumpolar ocean model driven by the same AOGCM as here. In this paper, we focus on the response of basal melt rate to a changing climate by retaining the same configuration of the Antarctic ice shelf as in the present day. To investigate the underlying mechanisms that determine the response of basal melting, we conduct sensitivity experiments by applying atmospheric and oceanic boundary conditions derived from the AOGCM individually. We analyze the responses of multiple ice shelves from West to East Antarctica to the climatic conditions and discuss the mechanisms determining basal mass balance change for different locations.

The paper is organized as follows. In section 2, the models and experiments are described. In section 3, we present the results of the (a) control (CTL) experiment, (b) LGM and $2\times CO_2$ experiments, and (c) sensitivity experiments under individual climatic forcing. Discussions and conclusions are given in section 4.

2. Model description and experimental design

a. *Model description of the Circumpolar Ocean Model*

We used a circumpolar ocean model to resolve the Antarctic ice shelf cavities (Kusahara and Hasumi 2013, 2014) based on the Center for Climate System Research (CCSR) Ocean Component Model (COCO; Hasumi 2006), which includes dynamic and thermodynamic sea ice. The model domain encompassed the Southern Hemisphere and an artificial northern boundary was set near 35°S (lower-left inset of Fig. 1). The model did not calculate ocean circulation to the north of the boundary. Horizontal resolution was about 10–20 km along the Antarctic coast. The heat and freshwater fluxes at the ice shelf–ocean interface were computed using a three-equation scheme (Hellmer and Olbers 1989; Holland and Jenkins 1999). This scheme diagnoses the heat and freshwater fluxes at the ice–ocean interface using temperature and salinity below the ice shelf prescribed from ocean model grids. By introducing an ice–ocean interface boundary layer between the ice shelf and the ocean, the upward heat flux Q_M^T and salt flux Q_M^S from the ocean to the boundary layer can be parameterized with a bulk formulation:

$$Q_M^T = -\rho c_p \gamma_t (T_b - T_m), \tag{1}$$

$$Q_M^S = \rho \gamma_s (S_b - S_m), \tag{2}$$

where ρ is the density of seawater (1028 kg m^{-3}); c_p is the specific heat capacity of seawater (4200 J kg^{-1} K^{-1}); $\gamma_t = 1.0\times10^{-4}$ m s^{-1} and $\gamma_s = 5.05\times10^{-7}$ m s^{-1} are constant thermal and salinity exchange velocities, respectively; T_b and S_b are the temperature and salinity at the ice–ocean interface boundary layer, respectively; and T_M and S_M are the temperature and salinity of the ocean model grid beneath the ice shelf base, respectively. We set Q_I^T as the conductive heat flux

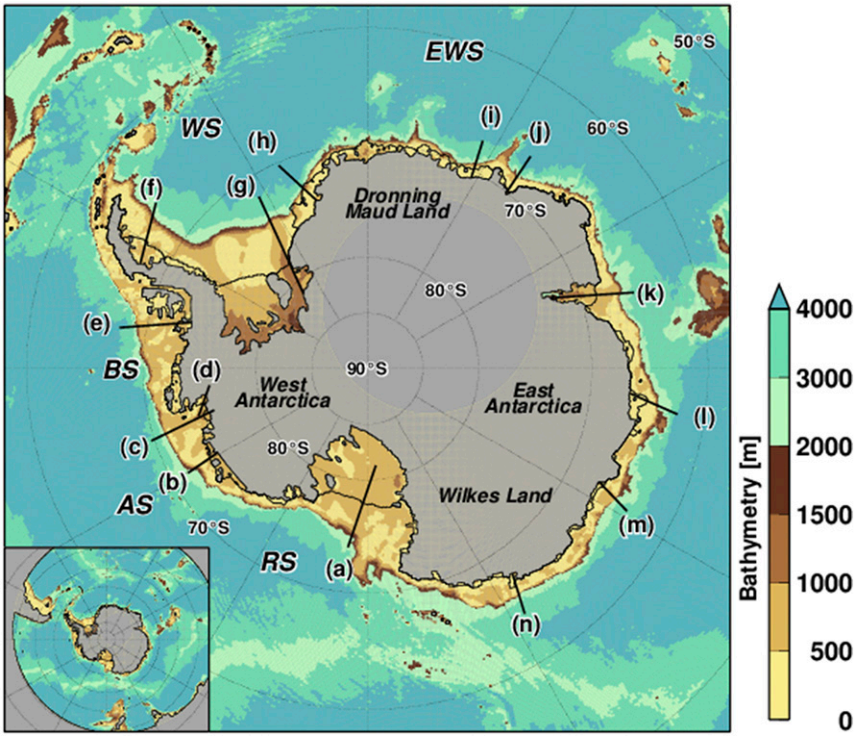

FIG. 1. Bottom topography used in the circumpolar ocean model. The model domain is indicated by the lower-left inset. Ocean temperature and salinity are restored to monthly climatology in the columns of the northernmost six grids. Solid black lines show the locations of the cross sections of the ocean profiles displayed in Figs. 9 and 14. WS indicates the Weddell Sea, EWS the eastern Weddell Sea, RS the Ross Sea, AS the Amundsen Sea, and BS the Bellingshausen Sea.

through the ice shelf (upward is positive). Therefore, $Q_I^T - Q_M^T$ represents the heat used in ice shelf melting, such that

$$Q_I^T - Q_M^T = -\rho w_b L \quad \text{and} \tag{3}$$

$$Q_I^S - Q_M^S = -\rho w_b S_b, \tag{4}$$

where w_b is the meltwater flux due to ice shelf melting and L is the latent heat of fusion (3.34×10^5 J kg^{-1}). The value of Q_I^T is estimated by assuming a constant vertical advection and diffusion (Holland and Jenkins 1999). Here, $Q_I^S = 0$ because no salinity flux exists within the ice shelf. Temperature at the ice shelf–ocean interface (T_b) is maintained at the freezing point of seawater. We use a linearized version of the equation of the freezing point of seawater, which depends on salinity and ocean depth (Mellor and Kantha 1989). Freshwater flux due to ice shelf melting or seawater freezing w_b can be computed using simultaneous equations on T_b, S_b, and w_b. Basal melt rate w_b is determined largely by the term representing the temperature gradient between the seawater and the ice shelf ($T_b - T_M$). The model does not calculate the dynamic and thermodynamic change in the ice shelves.

b. Description of the AOGCM experiments

We used the MIROC 4m AOGCM, which is based on MIROC 3.2 (Hasumi and Emori 2004). The MIROC 3.2 contributed to the Coupled Model Intercomparison Project phase 3, which was extensively cited in the Intergovernmental Panel on Climate Change Fourth Assessment Report. The coefficient of the isopycnal layer thickness diffusivity was 7.0×10^{-6} cm^2 s^{-1} instead of the value of 3.0×10^{-6} cm^2 s^{-1} used in the original MIROC 3.2 (Oka et al. 2011; Chikamoto et al. 2012). The resolution of the atmospheric component was T42 (about 2.8° × 2.8°) with 20 vertical levels, and that of the ocean component was about 1.4° × 1° with 43 vertical levels. Preindustrial boundary conditions were prescribed in the CTL experiment (e.g., an atmospheric CO_2 concentration of 285 ppm). The LGM experiment followed the protocol of PMIP2 (Braconnot et al. 2007) in which greenhouse gas concentrations (CO_2 value of 185 ppm) and global LGM ice sheet topography

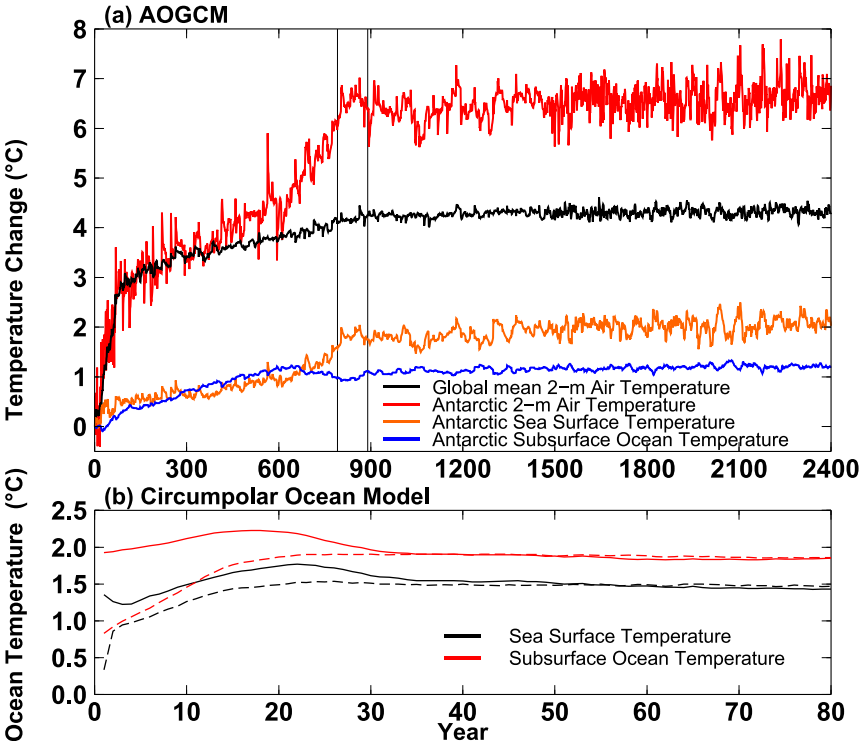

FIG. 2. Time series of the (top) $2\times CO_2$ AOGCM and (bottom) circumpolar ocean model experiments. At top, anomalies (from CTL) of global mean 2-m air temperature, Antarctic 2-m air temperature (65°–90°S), and Antarctic sea surface and subsurface ocean temperatures (south of 65°S, averaged over depths of 200–1000 m) are displayed. The climatology of years 791–890 (indicated by two thin vertical gray lines) is analyzed and used. At bottom, annual mean sea surface and subsurface (south of 60°S, 200–1000-m depth) temperatures for the circumpolar ocean model are shown. The dashed line is initialized with present-day ocean temperature and salinity fields, and the solid lines are initialized with $2\times CO_2$ ocean temperature and salinity fields derived from the AOGCM experiments.

were prescribed (Kawamura et al. 2017). In the $2\times CO_2$ experiment, we increased the atmospheric CO_2 concentration by 1% compound per year from the preindustrial value (285 ppm) until it doubled (571 ppm, at the 70th year) and the value was held constant thereafter (Yamamoto et al. 2015; Yoshimori et al. 2016). Based on the representative concentration pathway (RCP), CO_2 concentration reaches a value of 538 ppm at 2100 for RCP 4.5 and 571 ppm at mid-2050 for RCP 8.5. The model was integrated for 3800 years for the CTL and 2300 years for the LGM to reach respective quasi-steady states. The climatologies of the AOGCM experiments for 100 years from the quasi-equilibrium states were adopted for the analysis and used as boundary conditions for the circumpolar ocean model experiments. In the case of the $2\times CO_2$ experiment, we took the climatology from the years 791–890, when the sea surface and subsurface ocean temperatures in the Southern Ocean reached quasi-equilibrium, as shown in Fig. 2a. While more than 70% of the increase of global mean surface air temperature is accomplished within 200 years, the increases of surface and ocean temperature in the Southern Ocean do not even reach half the final value of change during the same period (Fig. 2a). This is because of the thermal inertia of the Southern Ocean (Manabe et al. 1990). The increase of sea surface temperature around years 700–800 is related to the recovery of deep convection in the Weddell Sea (Yamamoto et al. 2015).

The climatic fields simulated by the AOGCM experiments are displayed in Figs. 3 and 4. The simulated global mean annual 2-m air temperature anomaly to CTL for the LGM (−5.7°C) is consistent with previous reconstructions and other climate model results (Braconnot et al. 2012, Abe-Ouchi et al. 2015). The air temperature and ocean temperature from the surface to the bottom decrease in the Antarctic region (Fig. 3a) for the LGM conditions. The 2-m air temperature anomaly depends on the season (i.e., the magnitude of winter air temperature anomaly is

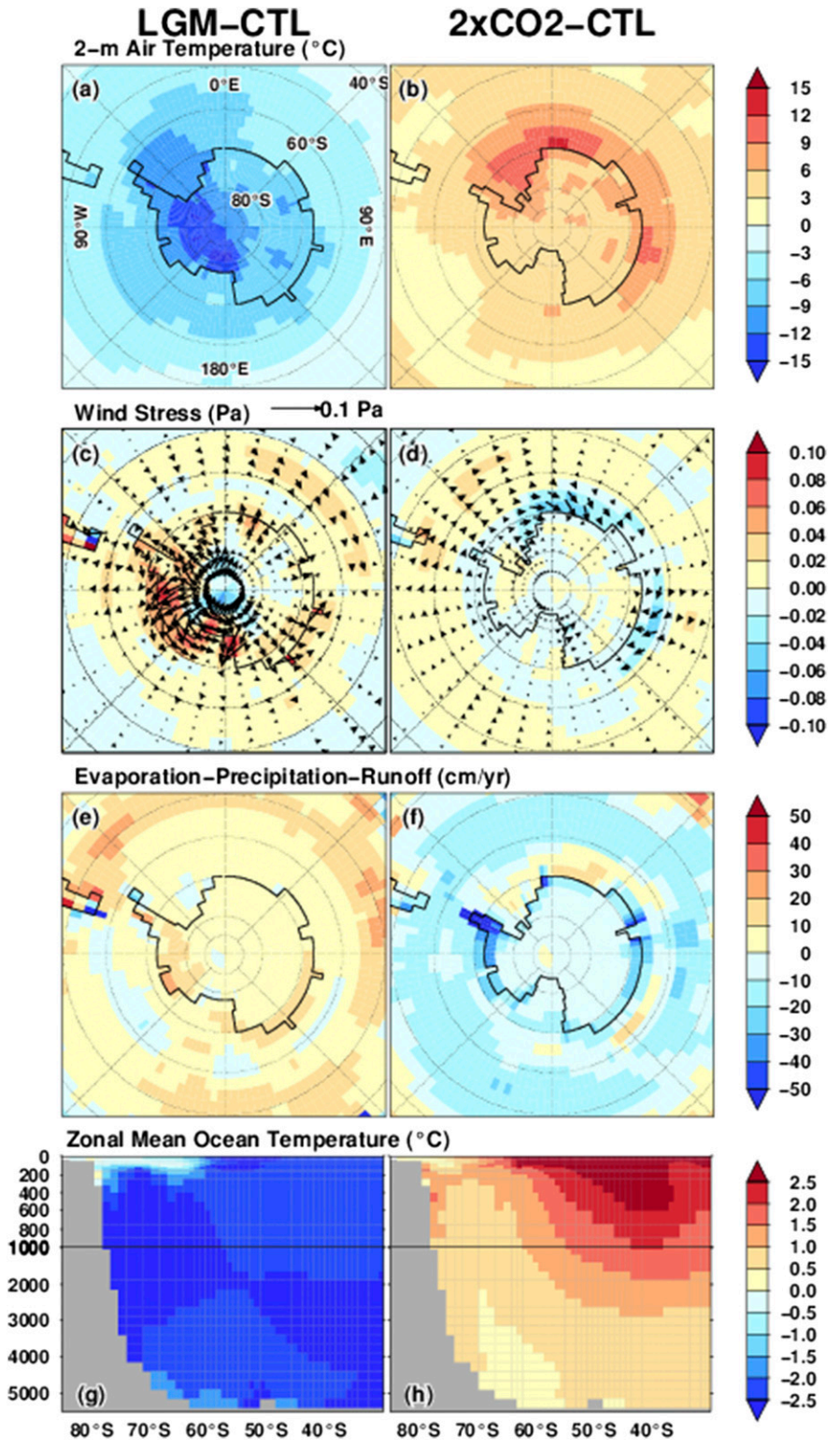

FIG. 3. Simulated climatic fields for (left) LGM and (right) $2\times CO_2$ in the AOGCM experiments (anomaly from the CTL experiment). (a),(b) 2-m air temperature; (c),(d) surface wind stress (positive value indicates stronger wind stress); (e),(f) sea surface freshwater flux due to evaporation, precipitation, and river runoff (positive value indicates net precipitation decrease); and (g),(h) zonal mean ocean temperature in the Southern Hemisphere. Note that we take the 100-yr mean climatology of model years 791–890 for the $2\times CO_2$.

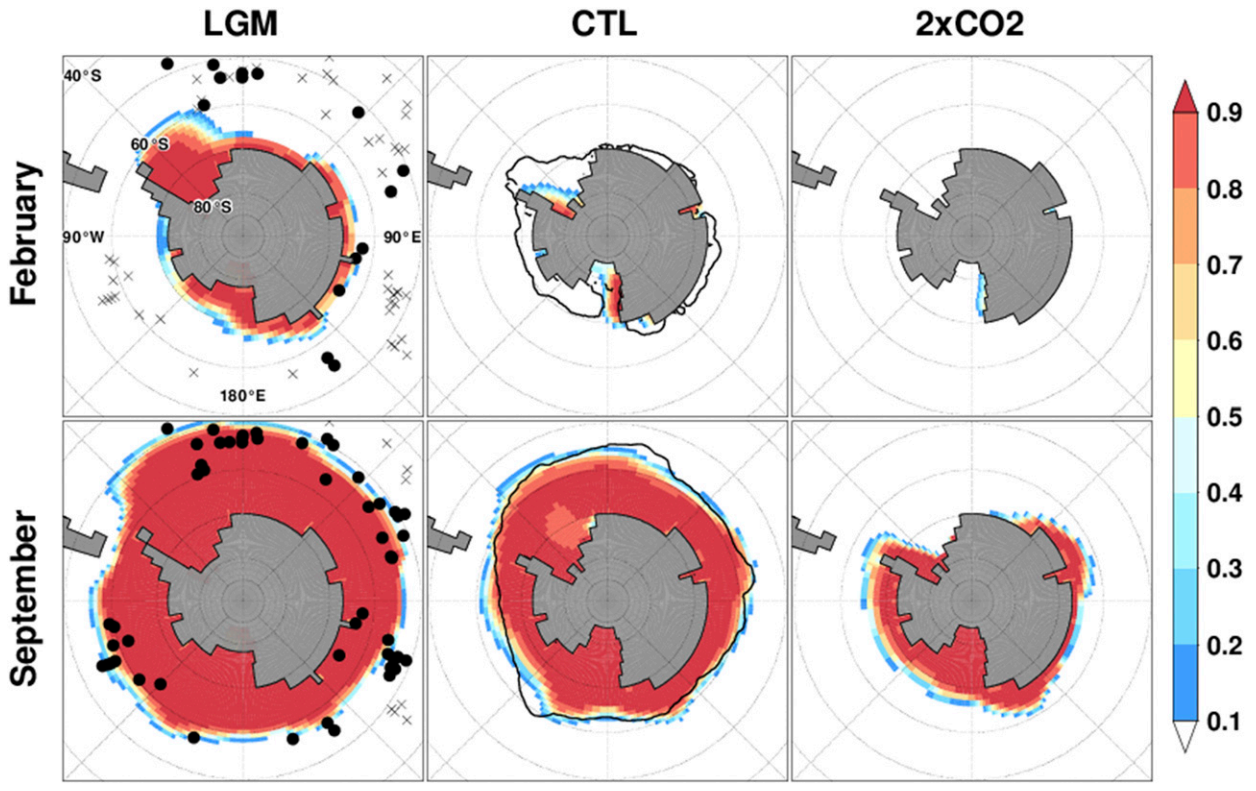

FIG. 4. Simulated sea ice concentration from the AOGCM for (left to right) LGM, CTL, and 2×CO_2. Black dots (presence of sea ice) and crosses (areas free of sea ice) on the panels of LGM experiments denote the reconstructions (Gersonde et al. 2005; Waelbroeck et al. 2009). Black lines in the CTL experiments indicate the observed present-day sea ice edge, which is defined by a sea ice concentration of 15%, averaged for the period 1982–2011 (Reynolds et al. 2002).

larger than for summer). Sea ice extent during the LGM experiment (Fig. 4) is consistent with previous reconstructions (Gersonde et al. 2005; Waelbroeck et al. 2009), as analyzed in Roche et al. (2012). Decreased precipitation over the Antarctic region (Fig. 3e) during the LGM is consistent with other reconstructions (Parrenin et al. 2007). The katabatic wind from the Antarctic continent is intensified in the LGM experiment (Fig. 3c). The Southern westerly exhibits very little change in the LGM experiment, but precipitation in the Southern Ocean has shifted as in most of the AOGCMs (Rojas et al. 2009).

The simulated global annual mean 2-m air temperature anomaly to CTL in the 2×CO_2 experiment is 4.2°C (Fig. 3b), but in comparison the LGM experiment exhibits larger amplitudes of temperature change in the air and ocean temperature anomalies. As indicated by Fig. 4, the area of sea ice shrinks and sea ice cover in summer almost disappears. In the 2×CO_2 experiment, the westerly in the Southern Ocean shifts southward and this weakens the easterly wind along the Antarctic coast (Fig. 3d). Net precipitation over the Southern Ocean and Antarctica increases (Fig. 3f).

Focusing on the air and ocean temperatures in the Antarctic region, the 2-m air temperature anomaly averaged over the marine area of 65°–90°S is −8.1°C for the LGM and 6.7°C for the 2×CO_2 experiments. In contrast, the amplitude of sea surface temperature in the Antarctic region is smaller than the subsurface because of sea ice cover. For the CTL experiment, the Antarctic surface and subsurface (200–1000-m depth average) ocean temperatures are −1.2° and 1.7°C, respectively. Note that the subsurface ocean temperature (1.7°C) is warmer than the observation by 0.6°C. In the LGM experiment, surface and subsurface ocean temperatures drop by 0.6° and 2.8°C, respectively, whereas in the 2×CO_2 experiment, they increase by 1.5° and 0.9°C, respectively (Figs. 3g,h). The amplitude of the subsurface ocean temperature anomaly is much greater in the LGM in comparison with the 2×CO_2.

c. *Experimental design of the circumpolar ocean model*

The settings of the present-day (CTL) experiment for the circumpolar ocean model were the same as in Kusahara and Hasumi (2013). Daily atmospheric fields

TABLE 1. List of the circumpolar ocean model experiments. The names of the experiments are listed in the first column. The second to fifth columns denote the combinations of the atmospheric and ocean boundary conditions used in each of the experiments. The simulated amounts of basal melting of all Antarctic ice shelves and sea ice production within the Antarctic shelf seas (defined by the 1000-m isobath) are displayed in the final two columns. The parenthetical values in the sensitivity experiments indicate the contributions of each forcing, calculated from the ratio of the anomaly from the CTL [e.g., ($2\times CO_2$ATM − CTL) / ($2\times CO_2$ − CTL)].

Name	Atmospheric heat flux	Wind stress	Net precipitation	Ocean restoring	Total basal melt rate (Gt yr^{-1})	Sea ice production rate (1000 Gt yr^{-1})
CTL	CTL	CTL	CTL	CTL	830	6.77
LGM	LGM	LGM	LGM	LGM	556	10.97
$2\times CO_2$	$2\times CO_2$	$2\times CO_2$	$2\times CO_2$	$2\times CO_2$	2746	3.96
LGM_ATM	LGM	LGM	LGM	CTL	662 (61%)	10.27 (83%)
LGM_OCN	CTL	CTL	CTL	LGM	724 (39%)	7.03 (6%)
LGM_ATMHEAT	LGM	CTL	CTL	CTL	700 (47%)	8.54 (12%)
LGM_ATMWIND	CTL	LGM	CTL	CTL	1028 (−72%)	7.54 (18%)
LGM_ATMPRCP	CTL	CTL	LGM	CTL	850 (−7%)	6.81 (1%)
$2\times CO_2$_ATM	$2\times CO_2$	$2\times CO_2$	$2\times CO_2$	CTL	1864 (54%)	4.25 (90%)
$2\times CO_2$_OCN	CTL	CTL	CTL	$2\times CO_2$	1449 (32%)	6.13 (23%)
$2\times CO_2$_ATMHEAT	$2\times CO_2$	CTL	CTL	CTL	1819 (52%)	4.20 (91%)
$2\times CO_2$_ATMWIND	CTL	$2\times CO_2$	CTL	CTL	962 (7%)	6.64 (5%)
$2\times CO_2$_ATMPRCP	CTL	CTL	$2\times CO_2$	CTL	816 (−1%)	6.64 (5%)

derived from the ERA-15 reanalysis (Röske 2006) were used as sea surface boundary conditions. Ocean temperature and salinity columns in the northernmost six grid cells were restored to the monthly Polar Science Center Hydrographic Climatology (PHC; Steele et al. 2001) with a damping scale of 10 days. The ocean temperature and salinity fields were initialized with the PHC and ocean velocities as zero. The atmospheric and oceanic boundary conditions were modified in the LGM and $2\times CO_2$ experiments based on the results of the AOGCM experiments. The monthly mean anomalies of the LGM and $2\times CO_2$ experiments from the CTL simulation of the AOGCM were superimposed on the present-day atmospheric and oceanic boundary conditions used in the CTL experiment. This procedure was applied to minimize the biases of the AOGCM. Note that the identical present-day Antarctic ice sheet configuration was used in the circumpolar ocean model experiments to focus on the response of ice shelf melting. We initiated the LGM and $2\times CO_2$ experiments by applying two different initial ocean fields to investigate their dependence on the initial conditions and the time required to reach quasi-steady states. One experiment was initialized with ocean temperature and salinity fields from the PHC, and the other was initialized with the LGM or $2\times CO_2$ derived from the AOGCM. After 60 years of integration, the simulated basal melt rate and ocean temperature reached similar quasi-steady states (Fig. 2b). As the simulated basal melt rates exhibited spatial interannual variability, the final 20-yr averaged climatology was analyzed in all experiments.

d. *Design of sensitivity experiments for individual climatic forcing*

We conducted sensitivity experiments to separate the factors contributing to the changes in basal melt rate for the LGM and $2\times CO_2$ experiments (Table 1). The forcing of the ocean model constituted the ocean temperature and salinity forcing of the lateral boundary and sea surface atmospheric boundary conditions. Atmospheric boundary conditions comprised heat flux (sensible heat, latent heat, and radiative fluxes), sea surface momentum flux, and sea surface freshwater flux due to net precipitation. We named the sensitivity experiments using the terms ATM, OCN, ATMHEAT, ATMWIND, and ATMPRCP combined with LGM and $2\times CO_2$. The terms LGM_OCN and $2\times CO_2$_OCN denote that the ocean temperature and salinity at the lateral boundary were set to LGM or $2\times CO_2$, while other boundary conditions were set to CTL. Similarly, LGM_ATM and $2\times CO_2$_ATM denote that the atmospheric boundary conditions were set to LGM or $2\times CO_2$, while the ocean temperature and salinity at the lateral boundary were set to CTL. The terms ATMHEAT, ATMWIND, and ATMPRCP denote branches of the "ATM" experiments. ATMHEAT denotes that only atmospheric heat flux was set to LGM or $2\times CO_2$, while the other atmospheric boundary conditions as well as the oceanic boundary conditions were set to CTL. Similarly, ATMWIND and ATMPRCP denote that sea surface momentum flux and sea surface freshwater flux due to net precipitation, respectively, were set to LGM or $2\times CO_2$.

3. Results

a. Results of the CTL experiment

This section presents the results of the CTL experiments to compare the basal melting and oceanic structures with observations. The model in this study can approximately reproduce the spatial distribution of basal melt rate under the present-day climate (Kusahara and Hasumi 2013). Nevertheless, it should be noted that the basal melt rates of ice shelves in the Amundsen Sea are much smaller than observed (Figs. 5 and 6). This is because the warm water intrusion onto the Amundsen Sea continental shelf is too weak in the simulation. However, it has also been proposed that stronger sea ice production (Timmermann and Hellmer 2013) and insufficient horizontal resolutions of the circumpolar ocean model (Nakayama et al. 2014b) and atmospheric boundary conditions (Dinniman et al. 2015) could be responsible. The total rate of basal melting in Antarctica ($830\,\mathrm{Gt\,yr^{-1}}$) is less than the glaciological estimates of $1325 \pm 235\,\mathrm{Gt\,yr^{-1}}$ by Rignot et al. (2013) and $1454 \pm 174\,\mathrm{Gt\,yr^{-1}}$ by Depoorter et al. (2013). Subsurface ocean temperature is averaged over depths below 200 m to the seafloor for the Antarctic continental shelf seas (defined by the 1000-m isobath), and averaged over depths of 200 to 1000 m for the deep ocean (Fig. 5). The model exhibits a cold water mass above the Antarctic continental shelves and warm CDW outside the shelf break, consistent with observations. The model also indicates a Southern Ocean temperature that is colder by about 0.5°C compared with observations in many but not all regions. Sea ice extent (Fig. 7) and the spatial distribution of sea ice production rate (Fig. 8) reflect the observed characteristics of active sea ice production in the polynya areas along the Antarctic coast (Tamura et al. 2008).

Simulated basal melt rate, sea ice production, ocean temperature, and density structure from 14 transects around Antarctica are displayed in Fig. 9. The first basal melting mode, characterized by cold and dense shelf water (Jacobs et al. 1992), is reproduced in the Ross, Filchner-Ronne, and Amery ice shelves (Figs. 9a,g,k). The Ross Ice Shelf also has the characteristics of the third basal melting mode, as well as those of the first mode (Fig. 9a), because of the summer retreat of sea ice (Fig. 7). The second basal melting mode, characterized by the intrusion of warm CDW onto the continental shelves, is reproduced in the Bellingshausen Sea (Fig. 9e), whereas it is absent in the Amundsen Sea (Figs. 9c,d). The simulated water mass properties of the Amundsen Sea continental shelf resemble those of the first mode of basal melting. The features of a low basal melt rate and thermocline deepened toward the Antarctic coast are reproduced in the eastern Weddell Sea and in East Antarctica (Figs. 9h,i). The observed high melt rate in the Shackleton and Totten ice shelves (Rignot et al. 2013) suggests the intrusion of warm water, but the simulated intrusion of warm water is weak and the basal melt rate is small (Figs. 9l,m). Intrusion of warm subsurface water across the continental shelf break is simulated in the Totten Ice Shelf; however, a ridge in front of the ice appears to protect the ice shelf from warm water intrusion (Fig. 9m). Sea ice production near the Mertz glacier tongue is active but seasonal influences of warm subsurface water are simulated here (Fig. 9n). Cold ice shelf water originating from the Filchner-Ronne Ice Shelf flows near the Larsen C Ice Shelf causing low basal melting (Fig. 9f). To summarize, the vertical oceanic structure and basal melt rate in the CTL experiment are reproduced well, although there are some discrepancies at specific locations.

b. Results of the LGM and $2\times CO_2$ experiments

Sea ice distribution shows a northward shift in the LGM experiment (Fig. 7), which is consistent with reconstructions (Gersonde et al. 2005; Waelbroeck et al. 2009). Although the summer sea ice in the circumpolar ocean model exhibits a complex pattern, which is a side effect of driving the model using an AOGCM, it reproduces the sea ice proxies better than the AOGCMs, which often suffer from warm bias in the Southern Ocean, as discussed in Roche et al. (2012). The large loss of sea ice in the $2\times CO_2$ experiment is consistent with the results of the AOGCM (Figs. 4 and 7). The simulated total basal melt rates are $556\,\mathrm{Gt\,yr^{-1}}$ in the LGM and $2746\,\mathrm{Gt\,yr^{-1}}$ in the $2\times CO_2$ experiments. Hence, the total basal melt rate is reduced by 30% in the LGM experiment and increased by 230% in the $2\times CO_2$ experiment compared with the CTL. Spatial distributions of the basal melt rate (Fig. 6) indicate that its response depends on the region, but high rates of basal melting at the grounding lines and ice shelf fronts, and low rates of basal melting in the interior parts of the ice shelves are common features among all the experiments. In the LGM experiment, basal melting rates in the Bellingshausen Sea decline in comparison with the CTL because the intrusion of warm water onto the continental shelf is reduced in the LGM. Basal melting rates in the Amundsen Sea also decline because summertime warm water formation on the Antarctic coast is reduced in the LGM. However, strong basal melting at the grounding line of the Filchner-Ronne and Amery ice shelves remains because the ocean temperature near the ice shelf is already close to freezing point in the CTL experiment. In the $2\times CO_2$

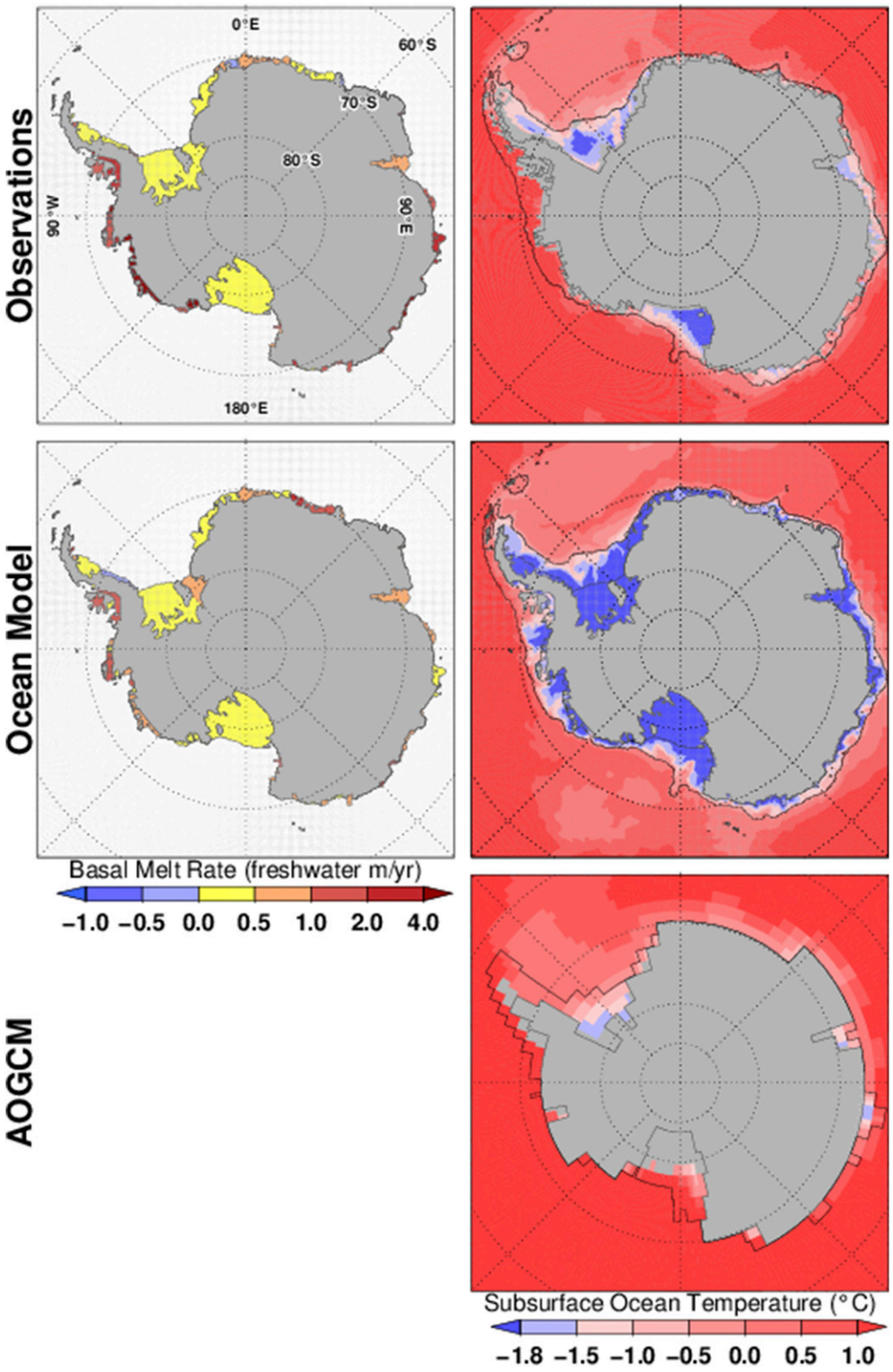

FIG. 5. (left) Comparison of observed and simulated basal melt rate for the ice shelves for the CTL experiment of the circumpolar ocean model. Observed basal melting rate is derived from Rignot et al. (2013). Basal melt rate is averaged within each ice shelf for comparison with Rignot et al. (2013). (right) Observed and simulated annual mean subsurface ocean temperatures in the circumpolar ocean model and AOGCM. Subsurface ocean temperature is averaged over depths below 200 m to the seafloor for the Antarctic continental shelf seas, and averaged over depths of 200 to 1000 m for the deep ocean. Black lines indicate the 1000-m isobath.

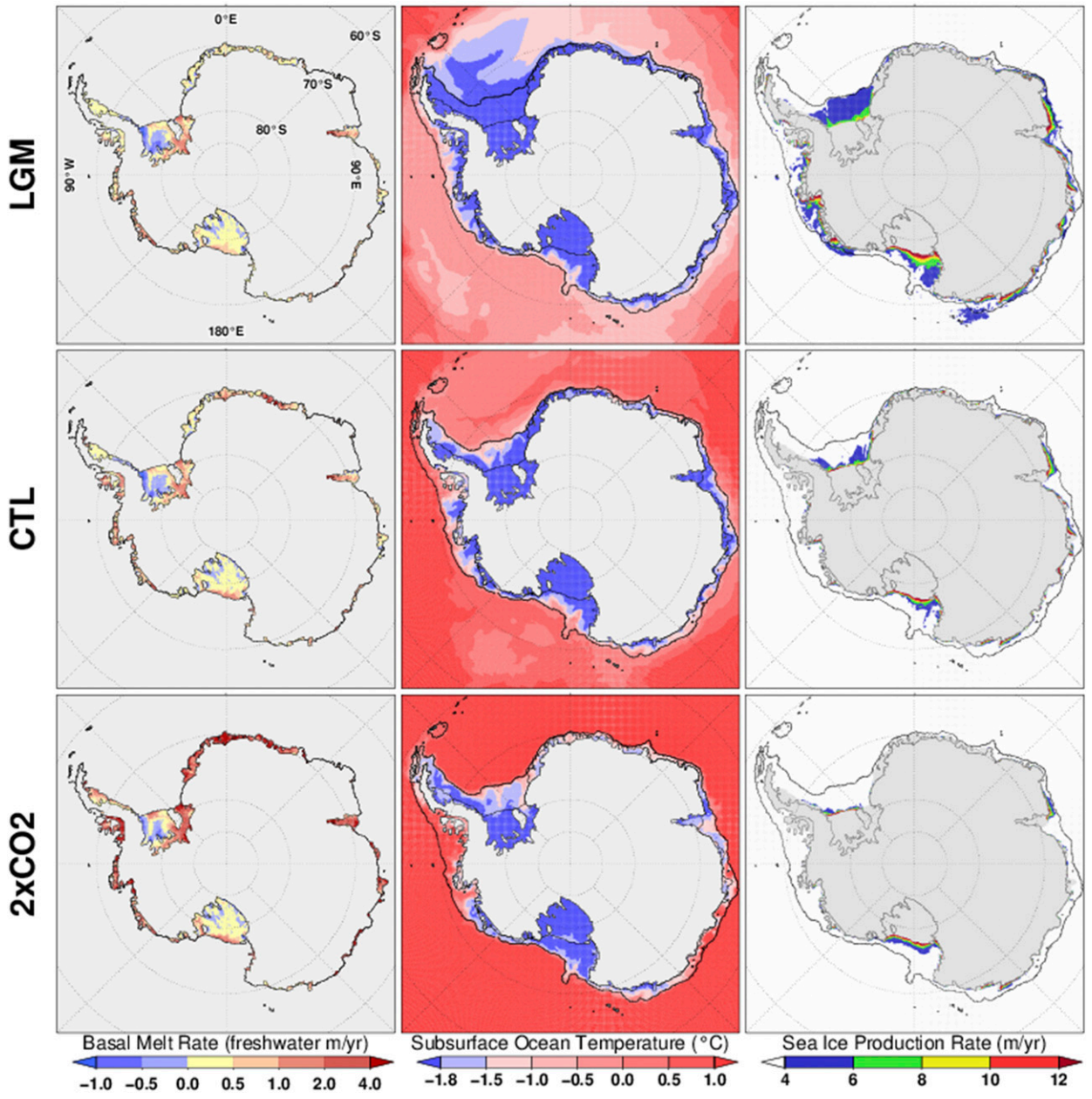

FIG. 6. (left) Simulated annual mean basal melt rate distribution (freshwater; m yr^{-1}); (middle) subsurface (averaged over depths of 200–1000 m) ocean temperature for the LGM, CTL, and $2\times CO_2$ experiments of the circumpolar ocean model; and (right) simulated sea ice production rate for which the color bar follows Tamura et al. (2008), displaying values >4 m yr^{-1}. Black lines indicate the 1000-m isobath.

experiment, many ice shelves experience drastic increases in basal melt rate in comparison with the CTL, but some ice shelves such as the Ross Ice Shelf do not. Summertime basal melting (January–March) constitutes 29%, 35%, and 40% of the annual basal melting in the LGM, CTL, and $2\times CO_2$ experiments, respectively, which indicates that seasonality in basal melting is intensified under a warmer climate (Fig. 10). As changes in the atmospheric fields influence heat loss at the sea surface, sea ice production increases in the LGM experiment and decreases in the $2\times CO_2$ experiment compared with the CTL (Fig. 6). Ocean temperature in the Southern Ocean offshore of the continental shelf break is reduced, but the reduction in ocean temperature along the continental shelf is small in most regions because it is already close to freezing point in the CTL

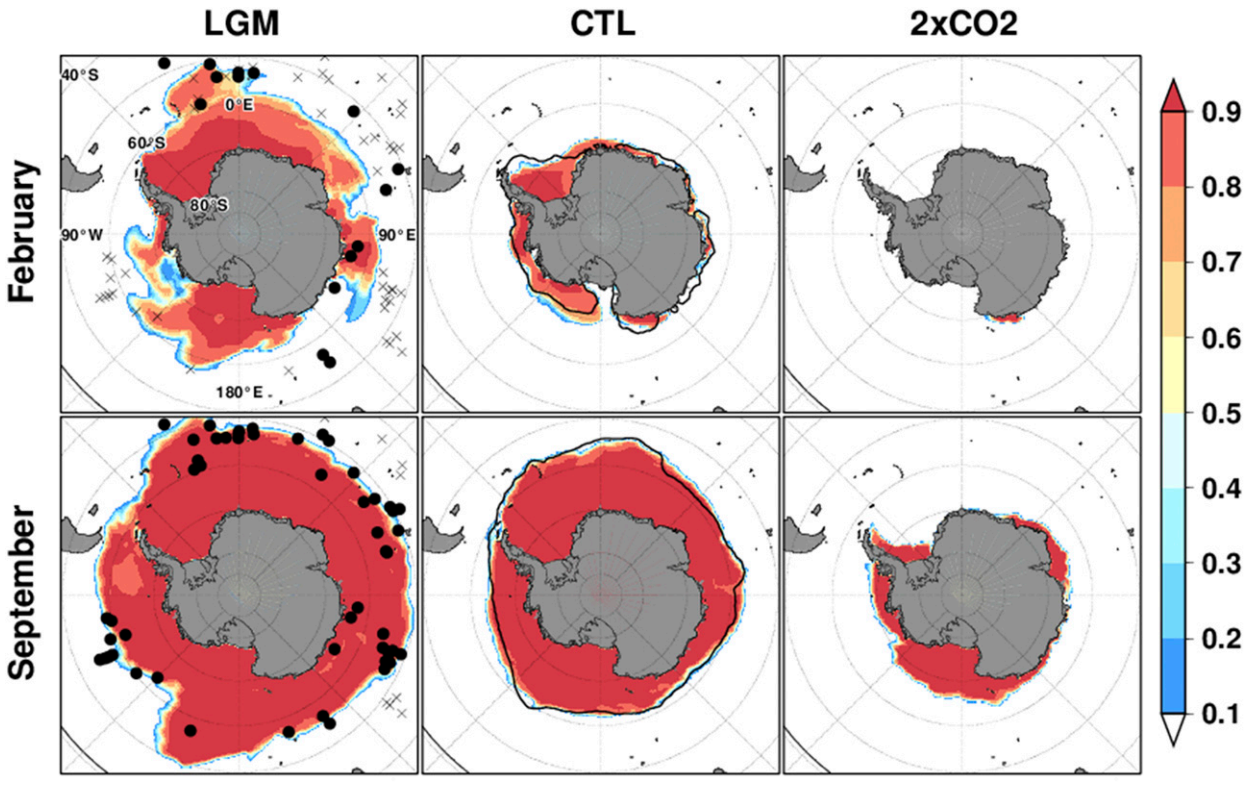

FIG. 7. As in Fig. 4 but for the circumpolar ocean model.

(Fig. 6). This feature is not evident in the AOGCM, suggesting that the AOGCM has limitations in representing water mass properties in shelf seas (Fig. 11). In the $2\times CO_2$ experiment, ocean temperature above the continental shelves of the Amundsen and Bellingshausen Seas increases in comparison with the CTL, where the basal melt rate increases drastically. In contrast, ocean temperature on the continental shelf does not increase in the Ross Sea.

Figure 9 indicates that the vertical oceanic structures in the shelf seas depend on climatic conditions. In the LGM experiment, the basal melt rate decreases in comparison with the CTL in the Bellingshausen Sea continental shelf area where cold shelf water is formed (Fig. 9e). Reduced summertime formation of surface warm water near the Ross Ice Shelf reduces the basal melt rate at the ice shelf front in the LGM experiment (Fig. 9a). In the $2\times CO_2$ experiment, cold and dense shelf water on the continental shelf is replaced with warm water, and the basal melt rate is increased in comparison with the CTL (Figs. 9c,d,k). The increase in subsurface water temperature leads to an increase in the basal melt rate in the Bellingshausen Sea where warm water intrusion already occurs in the CTL (Fig. 9e). The disappearance of sea ice cover during summer also contributes to the higher sea surface temperature and higher basal melt rate (Figs. 9f,i). In contrast, active sea ice production limits the intrusion of warm subsurface water beneath the Ross Ice Shelf and at the Mertz glacier tongue (Figs. 9a,n).

c. *Results of the sensitivity experiments under individual climatic forcing*

The simulated total basal melt rates of the sensitivity experiments are summarized in Fig. 12. It can be seen that nearly half the change in basal melting can be attributed to the change in atmospheric boundary conditions (ATM) and one-third can be attributed to the far-field oceanic boundary condition (OCN), which is mimicked by restoration changes at the northern boundary. The sum of the basal melt rate change in the OCN and ATM sensitivity experiments, displayed in Fig. 12 under the heading "SUM," indicates that the simulated change in basal melting is explained by the combination of oceanic and atmospheric boundary conditions. With regard to the atmospheric boundary conditions, the majority of basal melt rate change can be attributed to heat flux change. The contributions from wind and net precipitation changes are minor, with the exception of the opposite sign of the LGM wind. The increased basal melting in the LGM_ATMWIND experiment occurs because of enhanced northward sea ice

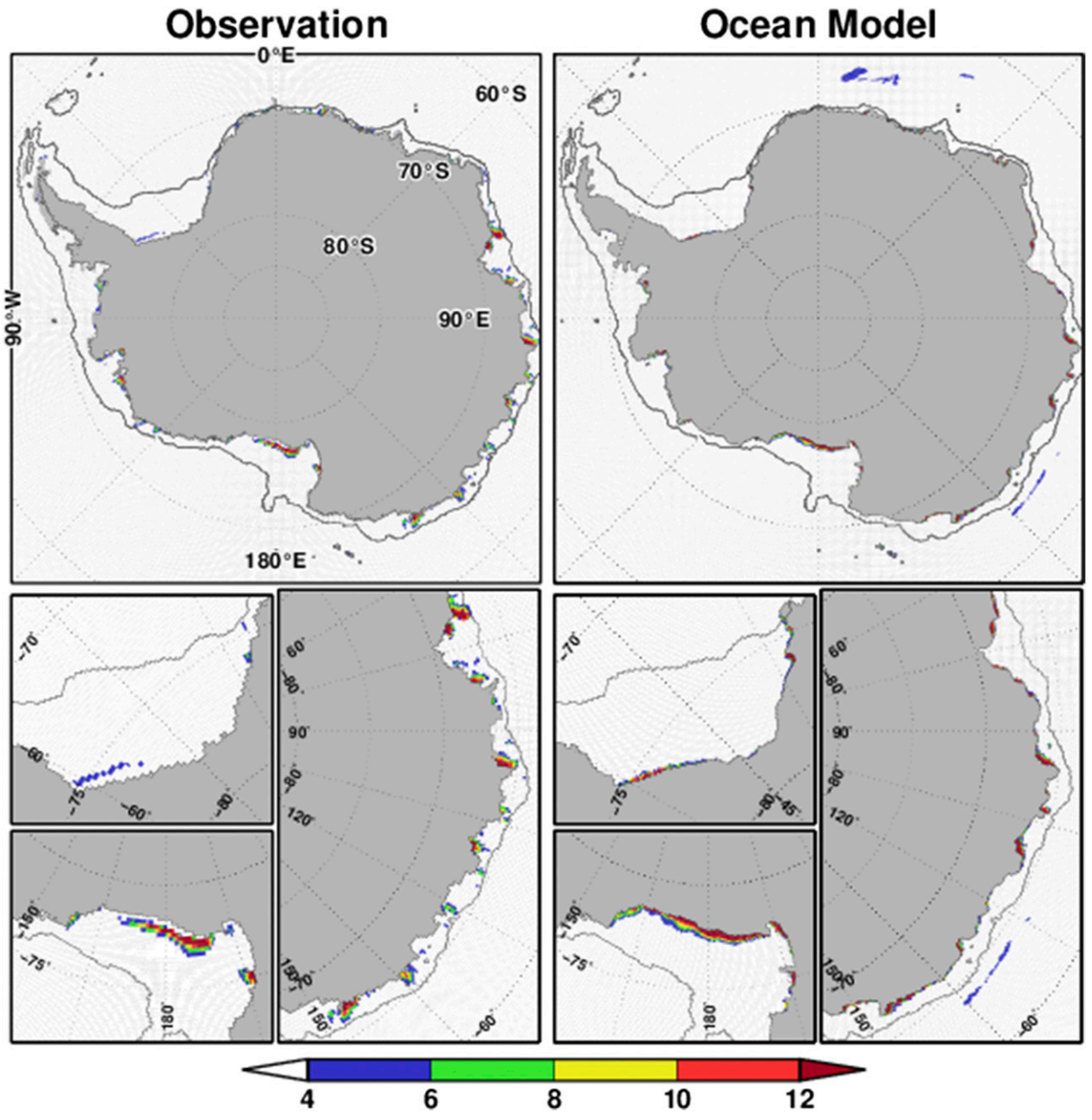

FIG. 8. (left) Observed sea ice production rate (sea ice; m yr^{-1}) derived from Tamura et al. (2008) and (right) simulated sea ice production rate in the CTL experiment of the circumpolar ocean model. Black contours indicate the 1000-m isobath. Bottom panels focus on sea ice production in three major polynya regions of the Weddell Sea, Ross Sea, and East Antarctica.

transport and sea ice decay during summer attributable to stronger katabatic winds directed to offshore along the Antarctic coast. This increases sea surface temperature and, thus, enhances basal melting. Conversely, in the LGM_ATM case, extensive sea ice remains along the Antarctic coast and the sea surface temperature is close to freezing point during summer because of the colder air temperature (Fig. 7). This means the effect of stronger wind on basal melt rate depends on the prevailing thermal condition, which is why the sum of LGM_ATMWIND and LGM_ATMHEAT is different from LGM_ATM. The impact of the $2\times CO_2$ wind change is relatively minor ($2\times CO_2$_ATMWIND) but it does increase the areal mean basal melting of the ice shelves of Dronning Maud Land where the easterly wind along the coast is weakened. The simulated changes in basal melt rate, subsurface ocean

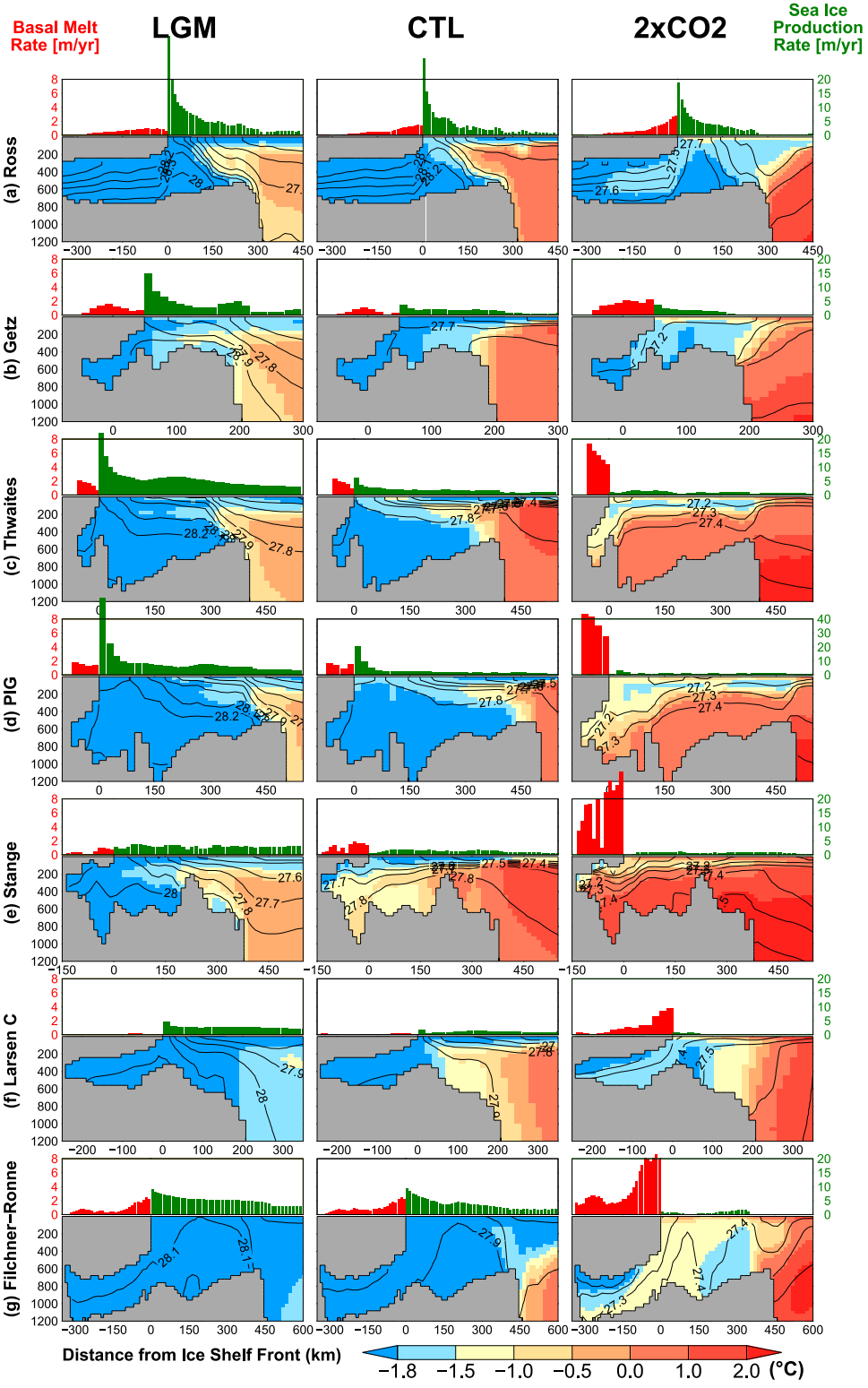

FIG. 9. Ocean transects from 14 ice shelves around Antarctica in the LGM, CTL, and 2×CO_2 experiments for the circumpolar ocean model. The lines denote the neutral density of seawater, and the colors denote ocean temperature. Basal melt rate (red bars above ice shelves) and sea ice production rate (green bars above open ocean) are displayed in the upper panels. The vertical axis denotes ocean depth and the horizontal axis denotes the distance from the ice shelf front. The locations of the transects are illustrated in Fig. 1.

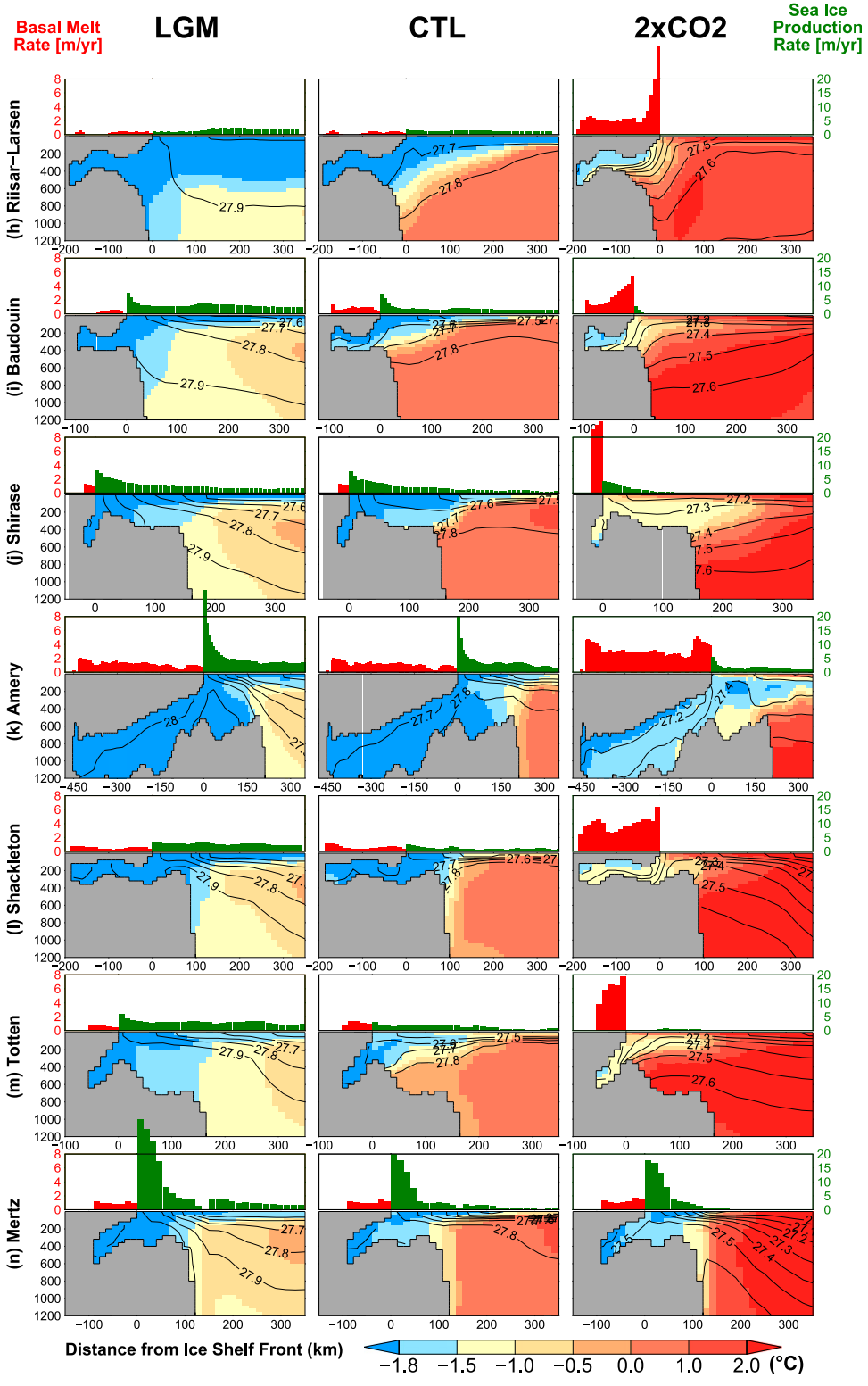

FIG. 9. (*Continued*)

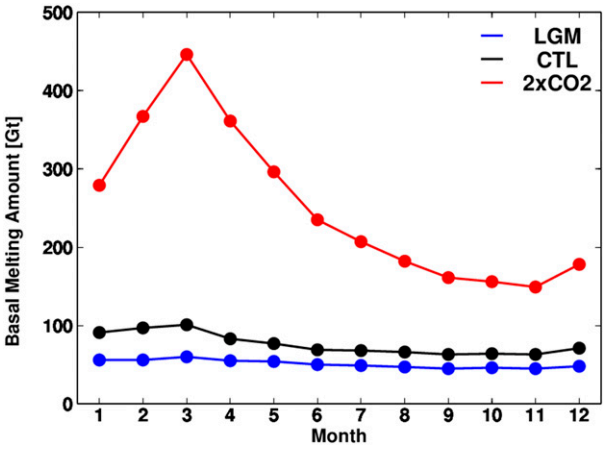

FIG. 10. Simulated basal mass loss of all Antarctic ice shelves for each month of the year for the circumpolar ocean model.

temperature, and sea ice production rate for the $2\times CO_2$ sensitivity experiments, attributable to the modification of the atmospheric heat flux ($2\times CO_2$_ATMHEAT) and oceanic boundary conditions ($2\times CO_2$_OCN), are displayed in Fig. 13. The contribution from net precipitation change is small. For sea ice production rate in the Antarctic shelf seas, sea surface thermal forcing (90%; Table 1) is the most important factor and the contribution from ocean forcing is minor (23%). Stronger offshore winds along the Antarctic coast in the LGM experiment contribute to increased sea ice production via enhanced sea ice transport and the maintenance of coastal polynyas.

The ocean transects from the sensitivity experiments are displayed in Fig. 14. While the change in atmospheric heat flux has small impact on the subsurface ocean temperature directly, it reduces sea ice production and promotes warm water intrusion onto the continental shelves in the Amundsen Sea (Figs. 14b–d). Warming in the far-field ocean temperature is insufficient to change the water mass properties in this region. The change in atmospheric heat flux reduces the sea ice extent and increases the sea surface temperature along the Antarctic coast during summer, which increases the areal mean basal melt rate in Dronning Maud Land and East Antarctica. This result indicates that changes in sea ice production and shelf water formation can affect the intrusion of warm water across the continental shelf break without any change in the ocean temperature offshore of the continental shelf break.

4. Discussion

Using a circumpolar ocean model forced by the output of a coupled climate model, we simulated the climatic conditions of the LGM and those associated with the doubling of atmospheric CO_2 to understand the response of the basal melt rate of the Antarctic ice shelves to long-term climatic change. In the CTL experiment, the temperature of the Antarctic shelf seas is close to the freezing point of seawater; nevertheless, warm water exists off the continental shelf break. This characteristic of ocean temperature difference across the continental shelf break is widely observed, and it is generated by active sea ice production and the formation of cold and dense shelf water that prevent the intrusion of warm water onto the continental shelves (Petty et al. 2013). The basal melting mode changes drastically in the $2\times CO_2$ simulation, where warm water intrusion onto continental shelves occurs in many places. This result is consistent with future projections (Hellmer et al. 2012; Timmermann and Hellmer 2013) that find warm water more able to intrude onto the continental shelves in a warmer climate. Hence, the responses of seawater temperature differ between the shelf sea and outside the continental shelf break. In addition, the basal melting mode characterized by the presence of thermocline deepening toward the continental shelf break disappears in the $2\times CO_2$ climate, as summer sea ice almost disappears. Stronger seasonality in basal melt rate (Fig. 10) reflects the higher summer sea surface temperature in the $2\times CO_2$ experiment, where summer sea ice cover vanishes along almost all the Antarctic coast (Fig. 7), while most of the Antarctic coast remains covered with sea ice in summer in the CTL experiment.

Subsurface ocean temperature is often used to parameterize the basal mass balance beneath ice shelves in ice sheet models (de Boer et al. 2015; Golledge et al. 2015; Sutter et al. 2016; Deconto and Pollard 2016). In the present study, the circumpolar ocean model is forced by the AOGCM output. Subsurface ocean temperature (1.7°C for CTL) decreases by −2.8°C for the LGM and it increases by 0.9°C for the $2\times CO_2$ experiments, indicating the amplitude of subsurface ocean temperature change is greater in the LGM compared with the $2\times CO_2$. This might reflect subsurface ocean temperatures in the AOGCM CTL experiment that are warmer (by about 0.6°C) compared with observations. Nevertheless, the rate of change of basal melt due to climate warming is much greater (by an order of magnitude) than that due to cooling. The results show that a change in basal melt rate is highly nonlinear in relation to the extent of changes in ocean temperature between colder and warmer climates. Water mass formation in the Antarctic shelf seas, associated with sea ice production and cold and dense shelf water formation, is critical to understanding the nonlinear response of ice shelf melting to changes in climate and ocean temperatures in the Antarctic region. One remark is that the

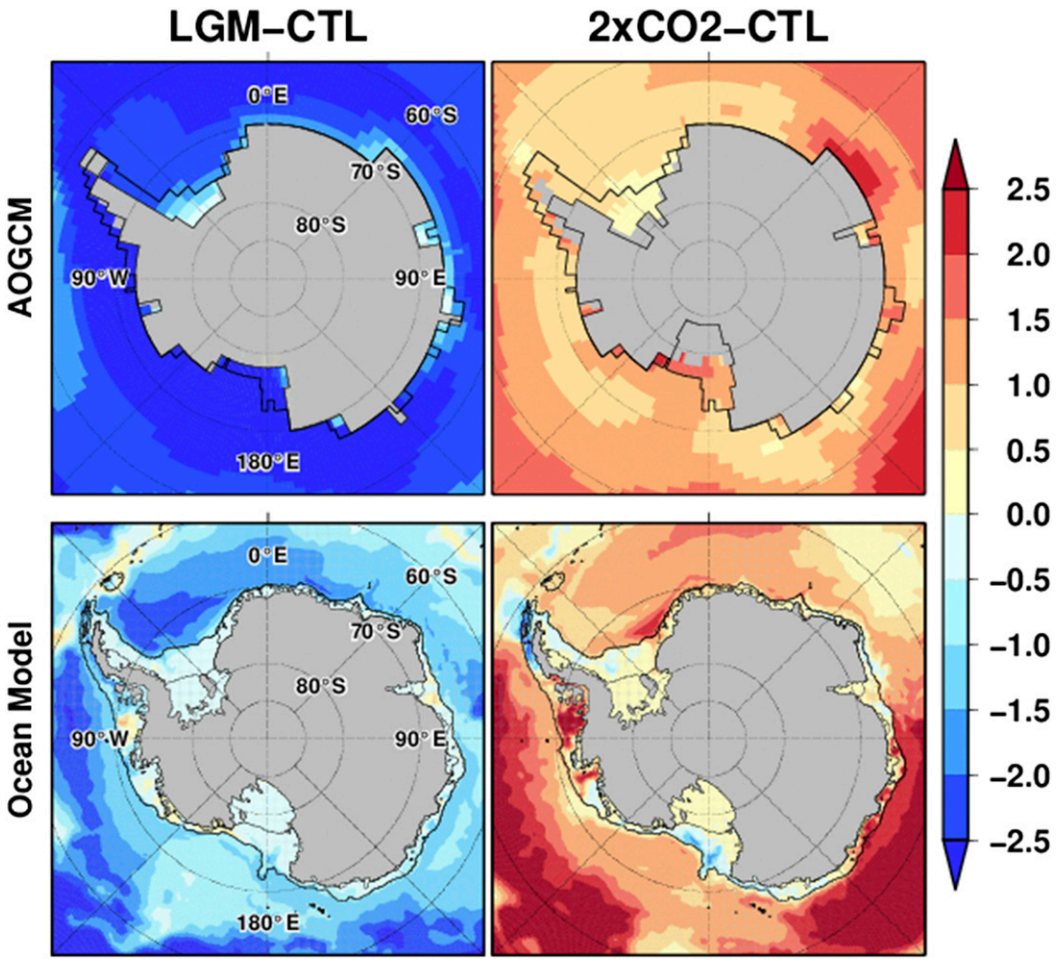

FIG. 11. Spatial distribution of annual mean subsurface ocean temperature (averaged over depths of 200–1000 m) anomaly (from the CTL) for the AOGCM and circumpolar ocean model experiments for LGM and $2\times CO_2$. Black lines indicate the 1000-m isobath of the AOGCM and the ocean model.

simulated intrusion of warm water onto the Amundsen Sea continental shelf is weak in the CTL experiment. Although this is a common problem for ocean models (Timmermann and Hellmer 2013), weak intrusion of warm water onto the Amundsen Sea continental shelf and strong sea ice production in the Amundsen Sea do not correspond with observations [at most $10\,m\,yr^{-1}$ in Tamura et al. (2008)]. These factors have to be improved in our model in future by adopting higher horizontal resolutions for the ocean model (Nakayama et al. 2014b) and for the atmospheric boundary conditions (Dinniman et al. 2015).

The sensitivity experiments that changed individual boundary conditions of the LGM or $2\times CO_2$ experiments were performed to investigate the mechanism of the response of basal melt rate to climate change. The results show that the majority of basal melt rate change can be explained by the thermal conditions of the atmosphere and the ocean, and that the impact of atmospheric heat flux is larger than that of subsurface ocean temperature change. The change in atmospheric heat flux plays a primary role in changing basal melt by changing the sea ice production rate and ocean structure. The changes in ocean structure, therefore, imply that climate influences the mode of basal melting, as proposed by Jacobs et al. (1992) and others. Although the far-field oceanic boundary condition changes the subsurface ocean temperature near the continental shelf break, it alone is insufficient to change sea ice production or the basal melting mode.

A long-term perspective is needed to understand the extent of the influence of anthropogenic activities on climate and sea level change (Clark et al. 2016). One essential difference between the transient future projection for the next few centuries (Hellmer et al. 2012; Timmermann and Hellmer 2013) and the quasi-equilibrium $2\times CO_2$ stems from the fact that the responses of the subsurface and deep ocean temperatures in the Southern Ocean are

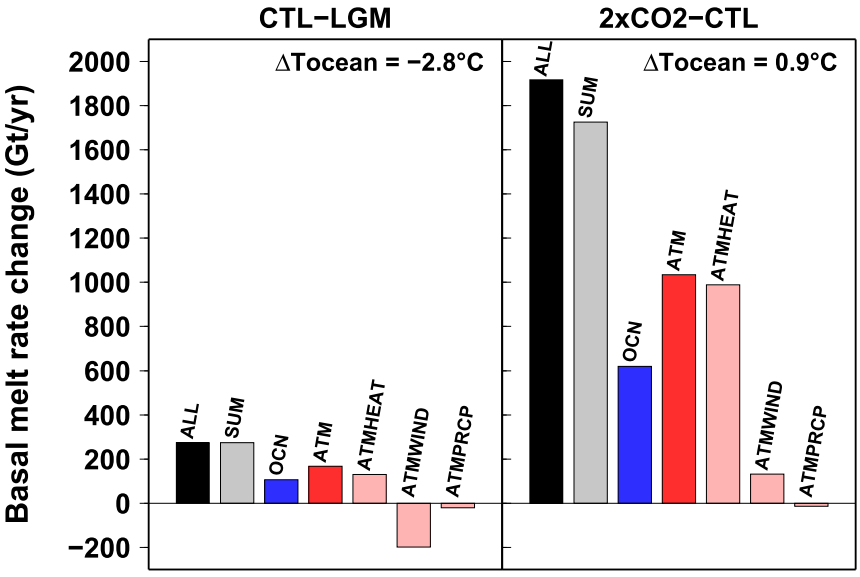

FIG. 12. Results of sensitivity experiments in Table 1 showing the response of total basal melt rate to the individual boundary conditions: (left) CTL − LGM and (right) $2\times CO_2$ − CTL. "ALL" denotes the LGM and $2\times CO_2$ experiments. "SUM" denotes the sum of the two sensitivity experiments of OCN and ATM, where OCN denotes the contributions of the far-field ocean boundary conditions, and ATM denotes the contributions of the atmospheric boundary conditions. The right three columns show the three components of the atmospheric boundary conditions that denote the contributions from atmospheric heat flux (ATMHEAT), sea surface momentum flux (ATMWIND), and net precipitation (ATMPRCP). ΔTocean denotes the subsurface ocean temperature anomaly in the Antarctic region simulated by the AOGCM experiments.

very slow. The response of the temperature of the deep Southern Ocean is delayed because of thermal inertia and deep convection, while the responses of the sea surface temperature and sea ice are relatively rapid (Yamamoto et al. 2015). Around years 700–800 in the $2\times CO_2$ AOGCM experiment (Fig. 2), the recovery of deep convection transports additional heat to the surface, which increases the sea surface and air temperatures, while cooling the subsurface ocean. As subsurface ocean temperature and the atmospheric conditions at the sea surface affect the basal melt rate, the temporal evolutions of the atmosphere and ocean could produce a complicated evolution of basal melt rate under future climate change.

From the sensitivity experiments, we find that wind affects the basal melt rate via several processes associated with sea ice and ocean currents, whose relative effectiveness depends on the prevailing thermal climatic conditions. In the LGM experiment, a stronger offshore katabatic wind enhances sea ice production and reduces the basal melt rate. Conversely, the LGM wind under the present-day warm climate increases the basal melt rate. This increase in basal melting occurs because of enhanced katabatic winds along the Antarctic coast that transport sea ice to north, which in turn increases the sea surface temperature during summer. Under a warmer climate, as in the $2\times CO_2$ experiment, the wind has little impact on basal melt. However, it does affect the basal melt rate along Dronning Maud Land, where the thermocline shoals toward the continental shelf, which is consistent with previous studies (Smedsrud et al. 2006; Hattermann et al. 2014; Spence et al. 2014).

Our study does not consider the effects of glacial meltwater and iceberg discharge into the Southern Ocean, which could warm the subsurface ocean by inducing stronger stratification and reducing vertical convection (Stouffer et al. 2007). Additional input of ice sheet meltwater could lead to increased basal melting because the Antarctic ice shelf is exposed to the warm ocean at such subsurface depths (Menviel et al. 2011; Nakayama et al. 2014a; Fogwill et al. 2015), while sea ice extent is increased (Bintanja et al. 2013, 2015; Pauling et al. 2016). Studies modeling ice sheets have shown that this subsurface warming could lead to a rapid retreat of the Antarctic ice sheet (Golledge et al. 2014). Thus, the interaction between the Antarctic ice sheet and the Southern Ocean could amplify the response of ice shelf melting to warmer climates.

We assumed a fixed configuration of the ice shelves in all of the experiments in order to focus on comprehending the role of climatic forcing in determining the basal

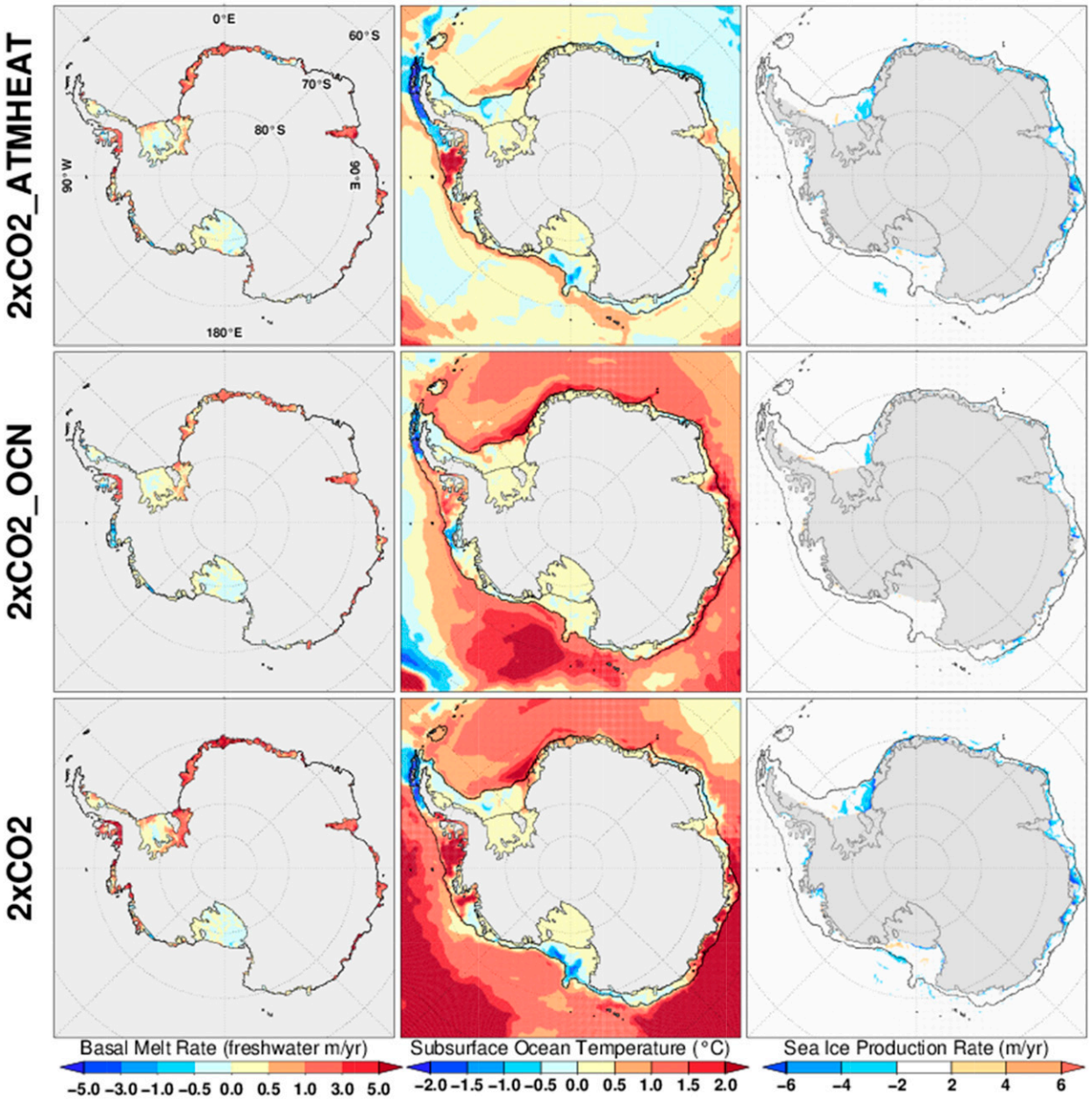

FIG. 13. Results of the $2\times CO_2$_ATMHEAT, $2\times CO_2$_OCN, and $2\times CO_2$ experiments. (left) Simulated annual mean basal melt rate anomaly (freshwater; m yr^{-1}; difference from CTL), (middle) subsurface (averaged over depths of 200–1000 m) ocean temperature anomaly, and (right) simulated sea ice production rate anomaly. Black lines indicate the 1000-m isobath.

melting of ice shelves. In reality, however, the changing basal mass balance actually modifies the thickness of the ice shelf and the positions of the grounding lines. This affects the sea ice and the ocean around the ice shelves, which in turn affect basal melting. With regard to the LGM experiments, reconstructions of the Antarctic ice sheet have shown that the grounding line would have advanced northward to near the continental shelf break during the LGM (Bentley et al. 2014; Abe-Ouchi et al. 2015). Using the same model as used in this study but with an enlarged LGM ice sheet extent, Kusahara et al. (2015) showed that basal melting during the LGM was greater than under the conditions of the present-day climate. This is because of the greater exposure of the ice shelves to the warmer subsurface water of the Southern Ocean as the grounding lines advanced toward the continental shelf breaks. This result is consistent with Abe-Ouchi et al. (2013), who found that the advance of the Laurentide ice

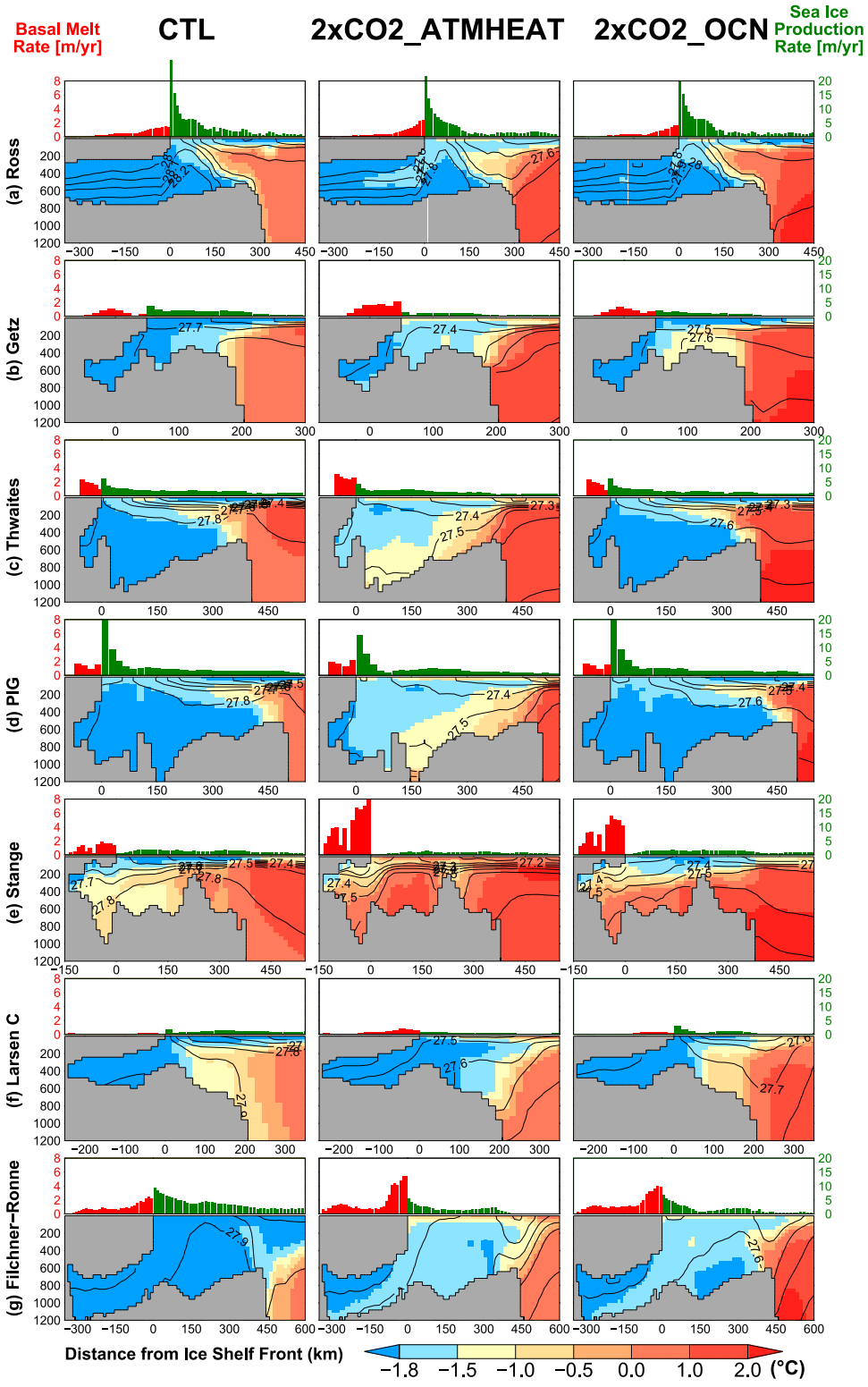

FIG. 14. As in Fig. 9, but for the CTL, 2×CO_2_ATMHEAT, and 2×CO_2_OCN experiments.

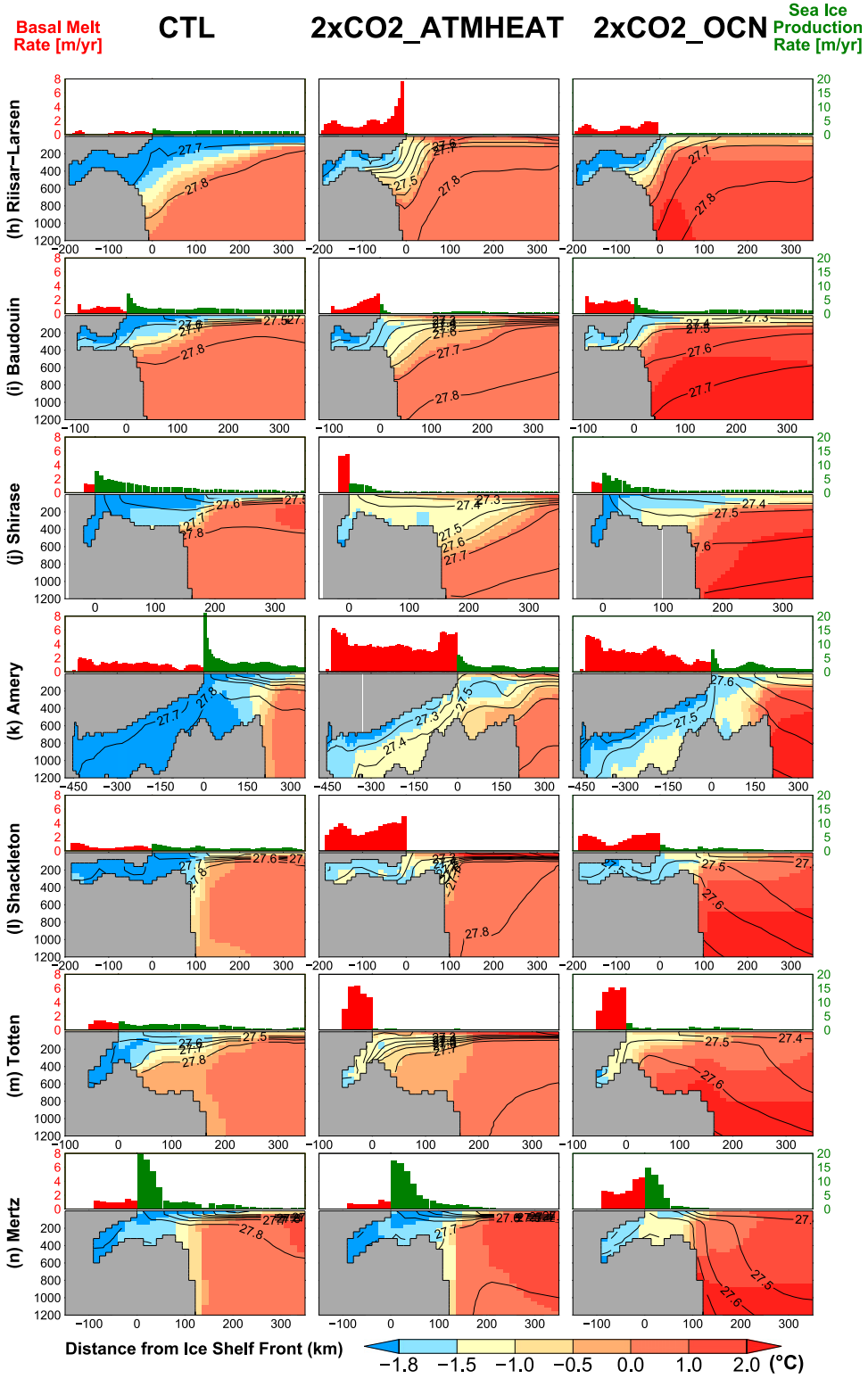

FIG. 14. (*Continued*)

sheet to lower latitudes leads to a negative mass balance for the ice sheet, which is essential to explain the ice age cycles. While the present study demonstrates the response of ice shelf melting to long-term climatic changes, the development of ice sheet–ocean coupling will be required to understand the changes of the Antarctic ice sheet (Kusahara 2016). Whether topographical changes of the Antarctic ice shelf have greater impact on the rate of ice sheet melting than climate change could depend on the prevailing background climate (i.e., colder or warmer than the present day). Coupling studies of ice sheet, ocean, and climate are therefore needed in future for investigating both glacial climate and future climate change.

In summary, our results derived from the LGM and CO_2 doubling experiments show the importance of atmosphere-driven water mass formation on basal melt rate, which generates a nonlinear response of basal melt rate to subsurface ocean temperature in the Antarctic region, originally simulated by the AOGCM. Cold and dense water mass formation in the Antarctic shelf seas due to sea ice production influences the intrusion of warm water onto the continental shelves, and reduced summer sea ice extent contributes to higher sea surface temperatures during summer. Our results demonstrate the importance of combining AOGCMs and ocean models that can resolve ice shelf cavity circulations to enhance our understanding of the responses of the Antarctic ice sheet to climate change.

Acknowledgments. We appreciate the work of the three anonymous reviewers whose comments helped us improve the manuscript. This research was supported by JSPS KAKENHI Grant 25241005 and the Environment Research and Technology Development Fund (S-10) of the Ministry of the Environment, Japan. We performed numerical simulations on the Oakleaf-FX at the University of Tokyo and the Earth Simulator at JAMSTEC.

REFERENCES

Abe-Ouchi, A., F. Saito, K. Kawamura, M. E. Raymo, J. Okuno, K. Takahashi, and H. Blatter, 2013: Insolation-driven 100,000-year glacial cycles and hysteresis of ice-sheet volume. *Nature*, **500**, 190–193, doi:10.1038/nature12374.

——, and Coauthors, 2015: Ice-sheet configuration in the CMIP5/PMIP3 Last Glacial Maximum experiments. *Geosci. Model Dev.*, **8**, 3621–3637, doi:10.5194/gmd-8-3621-2015.

Beckmann, A., and H. Goosse, 2003: A parameterization of ice shelf–ocean interaction for climate models. *Ocean Modell.*, **5**, 157–170, doi:10.1016/S1463-5003(02)00019-7.

Bentley, M. J., and Coauthors, 2014: A community-based geological reconstruction of Antarctic Ice Sheet deglaciation since the Last Glacial Maximum. *Quat. Sci. Rev.*, **100**, 1–9, doi:10.1016/j.quascirev.2014.06.025.

Bindschadler, R. A., and Coauthors, 2013: Ice-sheet model sensitivities to environmental forcing and their use in projecting future sea level (the SeaRISE project). *J. Glaciol.*, **59**, 195–224, doi:10.3189/2013JoG12J125.

Bintanja, R., G. J. van Oldenborgh, S. Drijfhout, B. Wouters, and C. Katsman, 2013: Important role for ocean warming and increased ice-shelf melt in Antarctic sea-ice expansion. *Nat. Geosci.*, **6**, 376–379, doi:10.1038/ngeo1767.

——, ——, and C. A. Katsman, 2015: The effect of increased fresh water from Antarctic ice shelves on future trends in Antarctic sea ice. *Ann. Glaciol.*, **56**, 120–126, doi:10.3189/2015AoG69A001.

Braconnot, P., and Coauthors, 2007: Results of PMIP2 coupled simulations of the mid-Holocene and Last Glacial Maximum—Part 1: Experiments and large-scale features. *Climate Past*, **3**, 261–277, doi:10.5194/cp-3-261-2007.

——, S. P. Harrison, M. Kageyama, P. J. Bartlein, V. Masson-Delmotte, A. Abe-Ouchi, B. Otto-Bliesner, and Y. Zhao, 2012: Evaluation of climate models using palaeoclimatic data. *Nat. Climate Change*, **2**, 417–424, doi:10.1038/nclimate1456.

Chikamoto, M. O., A. Abe-Ouchi, A. Oka, R. Ohgaito, and A. Timmermann, 2012: Quantifying the ocean's role in glacial CO_2 reductions. *Climate Past*, **8**, 545–563, doi:10.5194/cp-8-545-2012.

Church, J., and Coauthors, 2013: Sea level change. *Climate Change 2013: The Physical Science Basis*, T. F. Stocker et al., Eds., Cambridge University Press, 1137–1216.

Clark, P. U., and Coauthors, 2016: Consequences of twenty-first-century policy for multi-millennial climate and sea-level change. *Nat. Climate Change*, **6**, 360–369, doi:10.1038/nclimate2923.

Cook, C. P., and Coauthors, 2013: Dynamic behaviour of the East Antarctic ice sheet during Pliocene warmth. *Nat. Geosci.*, **6**, 765–769, doi:10.1038/ngeo1889.

de Boer, B., R. S. W. van de Wal, L. J. Lourens, R. Bintanja, and T. J. Reerink, 2013: A continuous simulation of global ice volume over the past 1 million years with 3-D ice sheet models. *Climate Dyn.*, **41**, 1365–1384, doi:10.1007/s00382-012-1562-2.

——, and Coauthors, 2015: Simulating the Antarctic ice sheet in the late-Pliocene warm period: PLISMIP-ANT, an ice-sheet model intercomparison project. *Cryosphere*, **9**, 881–903, doi:10.5194/tc-9-881-2015.

Deconto, R. M., and D. Pollard, 2016: Contribution of Antarctica to past and future sea-level rise. *Nature*, **531**, 591–597, doi:10.1038/nature17145.

Depoorter, M. A., J. L. Bamber, J. A. Griggs, J. T. M. Lenaerts, S. R. M. Ligtenberg, M. R. van den Broeke, and G. Moholdt, 2013: Calving fluxes and basal melt rates of Antarctic ice shelves. *Nature*, **502**, 89–92, doi:10.1038/nature12567.

Dinniman, M. S., J. M. Klinck, and W. O. Smith, 2011: A model study of Circumpolar Deep Water on the West Antarctic Peninsula and Ross Sea continental shelves. *Deep-Sea Res. II*, **58**, 1508–1523, doi:10.1016/j.dsr2.2010.11.013.

——, ——, L.-S. Bai, D. H. Bromwich, K. M. Hines, and D. M. Holland, 2015: The effect of atmospheric forcing resolution on delivery of ocean heat to the Antarctic floating ice shelves. *J. Climate*, **28**, 6067–6085, doi:10.1175/JCLI-D-14-00374.1.

Dupont, T. K., and R. B. Alley, 2005: Assessment of the importance of ice-shelf buttressing to ice-sheet flow. *Geophys. Res. Lett.*, **32**, L04503, doi:10.1029/2004GL022024.

Dutton, A., and K. Lambeck, 2012: Ice volume and sea level during the last interglacial. *Science*, **337**, 216–219, doi:10.1126/science.1205749.

——, and Coauthors, 2015: Sea-level rise due to polar ice-sheet mass loss during past warm periods. *Science*, **349**, 6244, doi:10.1126/science.aaa4019.

Fogwill, C. J., S. J. Phipps, C. S. M. Turney, and N. R. Golledge, 2015: Sensitivity of the Southern Ocean to enhanced regional Antarctic ice sheet meltwater input. *Earth's Future*, **3**, 317–329, doi:10.1002/2015EF000306.

Fretwell, P., and Coauthors, 2013: Bedmap2: Improved ice bed, surface and thickness datasets for Antarctica. *Cryosphere*, **7**, 375–393, doi:10.5194/tc-7-375-2013.

Gagliardini, O., G. Durand, T. Zwinger, R. C. A. Hindmarsh, and E. Le Meur, 2010: Coupling of ice-shelf melting and buttressing is a key process in ice-sheets dynamics. *Geophys. Res. Lett.*, **37**, L14501, doi:10.1029/2010GL043334.

Galton-Fenzi, B. K., J. R. Hunter, R. Coleman, S. J. Marsland, and R. C. Warner, 2012: Modeling the basal melting and marine ice accretion of the Amery Ice Shelf. *J. Geophys. Res.*, **117**, C09031, doi:10.1029/2012JC008214.

Gersonde, R., X. Crosta, A. Abelmann, and L. Armand, 2005: Sea-surface temperature and sea ice distribution of the Southern Ocean at the EPILOG Last Glacial Maximum—A circum-Antarctic view based on siliceous microfossil records. *Quat. Sci. Rev.*, **24**, 869–896, doi:10.1016/j.quascirev.2004.07.015.

Golledge, N. R., C. J. Fogwill, A. N. Mackintosh, and K. M. Buckley, 2012: Dynamics of the last glacial maximum Antarctic ice-sheet and its response to ocean forcing. *Proc. Natl. Acad. Sci. USA*, **109**, 16 052–16 056, doi:10.1073/pnas.1205385109.

——, L. Menviel, L. Carter, C. J. Fogwill, M. H. England, G. Cortese, and R. H. Levy, 2014: Antarctic contribution to meltwater pulse 1A from reduced Southern Ocean overturning. *Nat. Commun.*, **5**, 5107, doi:10.1038/ncomms6107.

——, D. E. Kowalewski, T. R. Naish, R. H. Levy, C. J. Fogwill, and E. G. W. Gasson, 2015: The multi-millennial Antarctic commitment to future sea-level rise. *Nature*, **526**, 421–425, doi:10.1038/nature15706.

Gong, Y., S. L. Cornford, and J. Payne, 2014: Modelling the response of the Lambert Glacier–Amery Ice Shelf system, East Antarctica, to uncertain climate forcing over the 21st and 22nd centuries. *Cryosphere*, **8**, 1057–1068, doi:10.5194/tc-8-1057-2014.

Hasumi, H., 2006: CCSR Ocean Component Model (COCO) version 4.0. Center for Climate System Research Rep. 25, University of Tokyo, 68 pp.

——, and S. Emori, 2004: K-1 coupled model (MIROC) description. K-1 Tech. Rep. 1, Center for Climate System Research, University of Tokyo, 34 pp.

Hattermann, T., O. A. Nøst, J. M. Lilly, and L. H. Smedsrud, 2012: Two years of oceanic observations below the Fimbul Ice Shelf, Antarctica. *Geophys. Res. Lett.*, **39**, L12605, doi:10.1029/2012GL051012.

——, L. Smedsrud, O. A. Nøst, J. Lilly, and B. Galton-Fenzi, 2014: Eddy-resolving simulations of the Fimbul Ice Shelf cavity circulation: Basal melting and exchange with open ocean. *Ocean Modell.*, **82**, 28–44, doi:10.1016/j.ocemod.2014.07.004.

Hellmer, H. H., 2004: Impact of Antarctic ice shelf basal melting on sea ice and deep ocean properties. *Geophys. Res. Lett.*, **31**, L10307, doi:10.1029/2004GL019506.

——, and D. J. Olbers, 1989: A two-dimensional model for the thermohaline circulation under an ice shelf. *Antarct. Sci.*, **1**, 325–336, doi:10.1017/S0954102089000490.

——, S. Jacobs, and A. Jenkins, 1998: Oceanic erosion of a floating Antarctic glacier in the Amundsen Sea. *Ocean, Ice, and Atmosphere: Interactions at the Antarctic Continental Margin*, S. S. Jacobs and R. F. Weiss, Eds., Amer. Geophys. Union, 83–99.

——, F. Kauker, R. Timmermann, J. Determann, and J. Rae, 2012: Twenty-first-century warming of a large Antarctic ice-shelf cavity by a redirected coastal current. *Nature*, **485**, 225–228, doi:10.1038/nature11064.

Holland, D. M., and A. Jenkins, 1999: Modeling thermodynamic ice–ocean interactions at the base of an ice shelf. *J. Phys. Oceanogr.*, **29**, 1787–1800, doi:10.1175/1520-0485(1999)029<1787:MTIOIA>2.0.CO;2.

——, and D. Holland, 2015: On the rocks: The challenges of predicting sea level rise. *Eos, Trans. Amer. Geophys. Union*, **96**, doi:10.1029/2015EO036667.

Holland, P. R., A. Jenkins, and D. M. Holland, 2008: The response of ice shelf basal melting to variations in ocean temperature. *J. Climate*, **21**, 2558–2572, doi:10.1175/2007JCLI1909.1.

Jacobs, S. S., R. G. Fairbanks, and Y. Horibe, 1985: Origin and evolution of water masses near the Antarctic continental margin: Evidence from H218O/H216O ratios in seawater. *Oceanology of the Antarctic Continental Shelf*, S. S. Jacobs, Ed., Amer. Geophys. Union, 59–85.

——, H. H. Helmer, C. S. M. Doake, A. Jenkins, and R. M. Frolich, 1992: Melting of ice shelves and the mass balance of Antarctica. *J. Glaciol.*, **38**, 375–387, doi:10.1017/S0022143000002252.

——, H. H. Hellmer, and A. Jenkins, 1996: Antarctic Ice Sheet melting in the southeast Pacific. *Geophys. Res. Lett.*, **23**, 957–960, doi:10.1029/96GL00723.

——, A. Jenkins, C. F. Giulivi, and P. Dutrieux, 2011: Stronger ocean circulation and increased melting under Pine Island Glacier ice shelf. *Nat. Geosci.*, **4**, 519–523, doi:10.1038/ngeo1188.

Jenkins, A., and S. Jacobs, 2008: Circulation and melting beneath George VI ice shelf, Antarctica. *J. Geophys. Res.*, **113**, C04013, doi:10.1029/2007JC004449.

Kawamura, K., and Coauthors, 2017: State dependence of climatic instability over the past 720,000 years from Antarctic ice-core records and climate modeling. *Sci. Adv.*, **3**, e1600446, doi:10.1126/sciadv.1600446.

Kopp, R. E., F. J. Simons, J. X. Mitrovica, A. C. Maloof, and M. Oppenheimer, 2009: Probabilistic assessment of sea level during the last interglacial stage. *Nature*, **462**, 863–867, doi:10.1038/nature08686.

Kusahara, K., 2016: Warming ocean erodes ice sheets. *Nat. Climate Change*, **6**, 22–23, doi:10.1038/nclimate2900.

——, and H. Hasumi, 2013: Modeling Antarctic ice shelf responses to future climate changes and impacts on the ocean. *J. Geophys. Res. Oceans*, **118**, 2454–2475, doi:10.1002/jgrc.20166.

——, and ——, 2014: Pathways of basal meltwater from Antarctic ice shelves: A model study. *J. Geophys. Res. Oceans*, **119**, 5690–5704, doi:10.1002/2014JC009915.

——, T. Sato, A. Oka, T. Obase, R. Greve, A. Abe-Ouchi, and H. Hasumi, 2015: Modelling the Antarctic marine cryosphere at the Last Glacial Maximum. *Ann. Glaciol.*, **56**, 425–435, doi:10.3189/2015AoG69A792.

Losch, M., 2008: Modeling ice shelf cavities in a *z* coordinate ocean general circulation model. *J. Geophys. Res.*, **113**, C08043, doi:10.1029/2007JC004368.

Manabe, S., K. Bryan, and M. J. Spelman, 1990: Transient response of a global ocean–atmosphere model to a doubling of atmospheric carbon dioxide. *J. Phys. Oceanogr.*, **20**, 722–749, doi:10.1175/1520-0485(1990)020<0722:TROAGO>2.0.CO;2.

Masson-Delmotte, V., and Coauthors, 2013: Information from paleoclimate archives. *Climate Change 2013: The Physical Science Basis*, T. F. Stocker et al., Eds., Cambridge University Press, 383–464.

McKay, R. M., P. J. Barrett, R. S. Levy, T. R. Naish, N. R. Golledge, and A. Payne, 2016: Antarctic Cenozoic climate history from sedimentary records: ANDRILL and beyond. *Philos. Trans. Roy. Soc. London*, **374A**, 20140301, doi:10.1098/rsta.2014.0301.

Mellor, G. L., and L. Kantha, 1989: An ice–ocean coupled model. *J. Geophys. Res.*, **94**, 10 937–10 954, doi:10.1029/JC094iC08p10937.

Mengel, M., and A. Levermann, 2014: Ice plug prevents irreversible discharge from East Antarctica. *Nat. Climate Change*, **4**, 451–455, doi:10.1038/nclimate2226.

——, J. Feldmann, and A. Levermann, 2015: Linear sea-level response to abrupt ocean warming of major West Antarctic ice basin. *Nat. Climate Change*, **6**, 71–74, doi:10.1038/nclimate2808.

Menviel, L., A. Timmermann, O. E. Timm, and A. Mouchet, 2011: Deconstructing the Last Glacial termination: The role of millennial and orbital-scale forcings. *Quat. Sci. Rev.*, **30**, 1155–1172, doi:10.1016/j.quascirev.2011.02.005.

Miller, M. D., J. F. Adkins, D. Menemenlis, and M. P. Schodlok, 2012: The role of ocean cooling in setting glacial southern source bottom water salinity. *Paleoceanography*, **27**, PA3207, doi:10.1029/2012PA002297.

Morales Maqueda, M. A., A. J. Willmott, and N. R. T. Biggs, 2004: Polynya dynamics: A review of observations and modeling. *Rev. Geophys.*, **42**, RG1004, doi:10.1029/2002RG000116.

Naish, T., and Coauthors, 2009: Obliquity-paced Pliocene West Antarctic ice sheet oscillations. *Nature*, **458**, 322–328, doi:10.1038/nature07867.

Nakayama, Y., R. Timmermann, C. B. Rodehacke, M. Schröder, and H. H. Hellmer, 2014a: Modeling the spreading of glacial melt water from the Amundsen and Bellingshausen Seas. *Geophys. Res. Lett.*, **41**, 7942–7949, doi:10.1002/2014GL061600.

——, ——, M. Schröder, and H. H. Hellmer, 2014b: On the difficulty of modeling Circumpolar Deep Water intrusions onto the Amundsen Sea continental shelf. *Ocean Modell.*, **84**, 26–34, doi:10.1016/j.ocemod.2014.09.007.

Nicholls, K. W., 1997: Predicted reduction in basal melt rates of an Antarctic ice shelf in a warmer climate. *Nature*, **388**, 460–462, doi:10.1038/41302.

Nøst, O. A., M. Biuw, V. Tverberg, C. Lydersen, T. Hattermann, Q. Zhou, L. H. Smedsrud, and K. M. Kovacs, 2011: Eddy overturning of the Antarctic Slope Front controls glacial melting in the eastern Weddell Sea. *J. Geophys. Res.*, **116**, C11014, doi:10.1029/2011JC006965.

Oka, A., A. Abe-Ouchi, M. O. Chikamoto, and T. Ide, 2011: Mechanisms controlling export production at the LGM: Effects of changes in oceanic physical fields and atmospheric dust deposition. *Global Biogeochem. Cycles*, **25**, GB2009, doi:10.1029/2009GB003628.

Parrenin, F., and Coauthors, 2007: 1-D-ice flow modelling at EPICA Dome C and Dome Fuji, East Antarctica. *Climate Past*, **3**, 243–259, doi:10.5194/cp-3-243-2007.

Pauling, A. G., C. M. Bitz, I. J. Smith, and P. J. Langhorne, 2016: The response of the Southern Ocean and Antarctic sea ice to freshwater from ice shelves in an Earth system model. *J. Climate*, **29**, 1655–1672, doi:10.1175/JCLI-D-15-0501.1.

Peltier, W. R., D. F. Argus, and R. Drummond, 2015: Space geodesy constrains ice age terminal deglaciation: The global ICE-6G-C (VM5a) model. *J. Geophys. Res. Solid Earth*, **120**, 450–487, doi:10.1002/2014JB011176.

Petty, A. A., D. L. Feltham, and P. R. Holland, 2013: Impact of atmospheric forcing on Antarctic continental shelf water masses. *J. Phys. Oceanogr.*, **43**, 920–940, doi:10.1175/JPO-D-12-0172.1.

Pollard, D., and R. M. DeConto, 2009: Modelling West Antarctic ice sheet growth and collapse through the past five million years. *Nature*, **458**, 329–332, doi:10.1038/nature07809.

Pritchard, H. D., R. J. Arthern, D. G. Vaughan, and L. A. Edwards, 2009: Extensive dynamic thinning on the margins of the Greenland and Antarctic ice sheets. *Nature*, **461**, 971–975, doi:10.1038/nature08471.

——, S. Ligtenberg, H. Fricker, D. Vaughan, M. van den Broeke, and L. Padman, 2012: Antarctic ice-sheet loss driven by basal melting of ice shelves. *Nature*, **484**, 502–505, doi:10.1038/nature10968.

Reynolds, R. W., N. A. Rayner, T. M. Smith, D. C. Stokes, and W. Wang, 2002: An improved in situ and satellite SST analysis for climate. *J. Climate*, **15**, 1609–1625, doi:10.1175/1520-0442(2002)015<1609:AIISAS>2.0.CO;2.

Rignot, E., and S. S. Jacobs, 2002: Rapid bottom melting widespread near Antarctic Ice Sheet grounding lines. *Science*, **296**, 2020–2023, doi:10.1126/science.1070942.

——, ——, J. Mouginot, and B. Scheuchl, 2013: Ice-shelf melting around Antarctica. *Science*, **341**, 266–270, doi:10.1126/science.1235798.

Roche, D. M., X. Crosta, and H. Renssen, 2012: Evaluating Southern Ocean sea-ice for the Last Glacial Maximum and preindustrial climates: PMIP-2 models and data evidence. *Quat. Sci. Rev.*, **56**, 99–106, doi:10.1016/j.quascirev.2012.09.020.

Rojas, M., and Coauthors, 2009: The southern westerlies during the last glacial maximum in PMIP2 simulations. *Climate Dyn.*, **32**, 525–548, doi:10.1007/s00382-008-0421-7.

Röske, F., 2006: A global heat and freshwater forcing dataset for ocean models. *Ocean Modell.*, **11**, 235–297, doi:10.1016/j.ocemod.2004.12.005.

Sato, T., and R. Greve, 2012: Sensitivity experiments for the Antarctic ice sheet with varied sub-ice-shelf melting rates. *Ann. Glaciol.*, **53**, 221–228, doi:10.3189/2012AoG60A042.

Schoof, C., 2006: A variational approach to ice stream flow. *J. Fluid Mech.*, **556**, 227–251, doi:10.1017/S0022112006009591.

——, 2007: Ice sheet grounding line dynamics: Steady states, stability, and hysteresis. *J. Geophys. Res.*, **112**, F03S28, doi:10.1029/2006JF000664.

Smedsrud, L. H., A. Jenkins, D. M. Holland, and O. A. Nøst, 2006: Modeling ocean processes below Fimbulisen, Antarctica. *J. Geophys. Res.*, **111**, C01007, doi:10.1029/2005JC002915.

Spence, P., S. M. Griffies, M. H. England, A. M. C. Hogg, O. A. Saenko, and N. C. Jourdain, 2014: Rapid subsurface warming and circulation changes of Antarctic coastal waters by poleward shifting winds. *Geophys. Res. Lett.*, **41**, 4601–4610, doi:10.1002/2014GL060613.

Steele, M., R. Morley, and W. Ermold, 2001: PHC: A global ocean hydrography with a high-quality Arctic Ocean. *J. Climate*, **14**, 2079–2087, doi:10.1175/1520-0442(2001)014<2079:PAGOHW>2.0.CO;2.

St-Laurent, P., J. M. Klinck, and M. S. Dinniman, 2013: On the role of coastal troughs in the circulation of warm Circumpolar Deep Water on Antarctic shelves. *J. Phys. Oceanogr.*, **43**, 51–64, doi:10.1175/JPO-D-11-0237.1.

Stouffer, R. J., D. Seidov, and B. J. Haupt, 2007: Climate response to external sources of freshwater: North Atlantic versus the Southern Ocean. *J. Climate*, **20**, 436–448, doi:10.1175/JCLI4015.1.

Suganuma, Y., H. Miura, A. Zondervan, and J. Okuno, 2014: East Antarctic deglaciation and the link to global cooling during the Quaternary: Evidence from glacial geomorphology and ^{10}Be surface exposure dating of the Sør Rondane Mountains, Dronning Maud Land. *Quat. Sci. Rev.*, **97**, 102–120, doi:10.1016/j.quascirev.2014.05.007.

Sutter, J., P. Gierz, K. Grosfeld, M. Thoma, and G. Lohmann, 2016: Ocean temperature thresholds for Last Interglacial West Antarctic Ice Sheet collapse. *Geophys. Res. Lett.*, **43**, 2675–2682, doi:10.1002/2016GL067818.

Talbot, M. H., 1988: Oceanic environment of George VI ice shelf, Antarctic Peninsula. *Ann. Glaciol.*, **11**, 161–164, doi:10.1017/S0260305500006480.

Tamura, T., K. I. Ohshima, and S. Nihashi, 2008: Mapping of sea ice production for Antarctic coastal polynyas. *Geophys. Res. Lett.*, **35**, L07606, doi:10.1029/2007GL032903.

Thoma, M., A. Jenkins, D. Holland, and S. Jacobs, 2008: Modelling Circumpolar Deep Water intrusions on the Amundsen Sea continental shelf, Antarctica. *Geophys. Res. Lett.*, **35**, L18602, doi:10.1029/2008GL034939.

Timmermann, R., and H. H. Hellmer, 2013: Southern Ocean warming and increased ice shelf basal melting in the twenty-first and twenty-second centuries based on coupled ice-ocean finite element modelling. *Ocean Dyn.*, **63**, 1011–1026, doi:10.1007/s10236-013-0642-0.

——, Q. Wang, and H. H. Hellmer, 2012: Ice shelf basal melting in a global finite element sea ice–ice shelf–ocean model. *Ann. Glaciol.*, **53**, 303–314, doi:10.3189/2012AoG60A156.

Velicogna, I., 2009: Increasing rates of ice mass loss from the Greenland and Antarctic ice sheets revealed by GRACE. *Geophys. Res. Lett.*, **36**, L19503, doi:10.1029/2009GL040222.

Waelbroeck, C. and Coauthors, 2009: Constraints on the magnitude and patterns of ocean cooling at the Last Glacial Maximum. *Nat. Geosci.*, **2**, 127–132, doi:10.1038/ngeo411.

Walker, R. T., T. K. Dupont, B. R. Parizek, and R. B. Alley, 2008: Effects of basal-melting distribution on the retreat of ice-shelf grounding lines. *Geophys. Res. Lett.*, **35**, L17503, doi:10.1029/2008GL034947.

Weertman, J., 1974: Stability of the junction of an ice sheet and an ice shelf. *J. Glaciol.*, **13**, 3–11, doi:10.1017/S0022143000023327.

Whitworth, T., A. H. Orsi, S. J. Kim, and W. D. Nowlin Jr., 1998: Water masses and mixing near the Antarctic Slope Front. *Ocean, Ice, and Atmosphere: Interactions at the Antarctic Continental Margin*, S. S. Jacobs and R. F. Weiss, Eds., Amer. Geophys. Union, 1–27.

Williams, M. M., I. R. C. Warner, and W. F. Budd, 1998: The effects of ocean warming on melting and ocean circulation under the Arnery Ice Shelf, East Antarctica. *Ocean, Ice, and Atmosphere: Interactions at the Antarctic Continental Margin*, S. S. Jacobs and R. F. Weiss, Eds., Amer. Geophys. Union, 75–80.

Yamamoto, A., A. Abe-Ouchi, M. Shigemitsu, A. Oka, K. Takahashi, R. Ohgaito, and Y. Yamanaka, 2015: Global deep ocean oxygenation by enhanced ventilation in the Southern Ocean under long-term global warming. *Global Biogeochem. Cycles*, **29**, 1801–1815, doi:10.1002/2015GB005181.

Yamane, M., Y. Yokoyama, A. Abe-Ouchi, S. Obrochta, F. Saito, K. Moriwaki, and H. Matsuzaki, 2015: Exposure age and ice-sheet model constraints on Pliocene East Antarctic ice sheet dynamics. *Nat. Commun.*, **6**, 7016, doi:10.1038/ncomms8016.

Yoshimori, M., T. Yokohata, and A. Abe-Ouchi, 2009: A comparison of climate feedback strength between CO_2 doubling and LGM experiments. *J. Climate*, **22**, 3374–3395, doi:10.1175/2009JCLI2801.1.

——, M. Watanabe, H. Shiogama, A. Oka, A. Abe-Ouchi, R. Ohgaito, and Y. Kamae, 2016: A review of progress towards understanding the transient global mean surface temperature response to radiative perturbation. *Prog. Earth Planet. Sci.*, **3**, 21, doi:10.1186/s40645-016-0096-3.